Contribution to a better understanding of long-term hydration, structuration and mechanical properties of slag based cementitious materials: Experimental and modeling approaches

Mohamad Ali Ahmad, Harifidy Ranaivomanana, Stéphanie Bonnet, Paul Buttin, Valérie L'hostis

Contribution to a better understanding of long-term hydration, structuration and mechanical properties of slag based cementitious materials: experimental and modeling approaches.

Mohamad ALI AHMAD[a,b,*], Harifidy RANAIVOMANANA[a], Stéphanie BONNET[a], Paul BUTTIN[b], Valérie L'HOSTIS[c]

[a] Nantes Université, Ecole Centrale Nantes, CNRS, GeM, UMR 6183 F-44600 Saint-Nazaire, France
[b] CEA, CEA Pays de la Loire, F-44340 Bouguenais, France
[c] CEA, Université Paris-Saclay, 91191 Gif-sur-Yvette, France
[*] Corresponding author: mohamad.ali-ahmad@univ-nantes.fr

Highlight

- Proposing a new hydration model for slag-blended cement
- Avrami's exponential model is used to describe the hydration kinetics
- Modified version of Kolani's stoichiometric laws describes the chemical reactions
- Cement porosity is influenced by clinker substitution with slag rate
- Analytical links between hydration and mechanical properties can be established

Abstract

Blast Furnace Slag (BFS), a by-product of the steelmaking process, can be used as a mineral addition in blended cement. In addition to reduce CO_2 emissions in the construction field, the use of BFS in cementitious materials also contributes to the improvement of their mechanical and durability properties. However, despite the numerous studies proposed in the literature about the hydration properties of BFS-blended cement, some aspects remain unclear, such as the influence of slag substitution rate on hydration kinetics and on the stoichiometry of hydrates formed and their impacts on both microstructural and mechanical properties. For these reasons, the present study aims firstly to better understand how BFS-blended cement hydrates based on a complete hydration model that considers both kinetics and chemical reactions. The only required input data are the formulation parameters (*i.e.* water-to-binder ratio (W/B), substitution rate of clinker by slag (f_s)), and curing. This study does not introduce the heat of hydration, which limits the validity of other existing models to short-term hydration. Analytical laws involving calibration parameters, which are assumed to vary with the substitution rate of clinker by slag, represent the hydration kinetics of clinker and slag while a stoichiometric approach is adopted to describe the chemical formation of hydrates. In order to calibrate and validate the parameters involved in the hydration model, four different cement paste mixes formulated with 0%, 30%, 50%, and 80% (by mass) of slag are studied in terms of hydration degrees and microstructure evolutions, and completed with data from the literature. The amounts of hydrated phases and those of dry densities, particularly at later ages, are well reproduced by the hydration model. Porous structure evolutions are also investigated in terms of partition between capillary and CSH gel pores by comparing the capillary porosity predicted by the model with the total porosity measured experimentally. Finally, predictive modeling of mechanical properties (compressive strength and Young modulus) of tested materials are finally proposed based on hydration model outputs. A good agreement between experimental and predicted data is observed.

Keywords

BFS-blended cement, hydration degree, microstructure, mechanical properties, hydration model, mechanical model.

1 Introduction

Blast Furnace Slag (BFS) is a non-metallic mineral by-product of iron production with various uses in

the construction field due to its beneficial properties. Several studies have focused on combining Portland cement with BFS replacement while retaining a beneficial effect on the overall behavior of the structure [1], [2]. Various advantages for using slag are reported in the literature and are related to low heat of hydration [3], [4], and high chloride resistance [5], [6]. In addition, studies show that slag cement improves the compressive strength and durability properties [7], [8], and then the corrosion initiation of the mixed material. The improved properties are related to the modified microstructure related to the different hydration reactions.

The main compounds of the BFS are silicate, alumina, and calcium, so its chemical composition is close to that of Ordinary Portland Cement (OPC). When slag is mixed with water, it hydrates, but at a very slow rate without an activator [2], [9]. Generally, a basic agent is always required to activate the slag; we distinguish essentially the alkaline activation, which can be sodium or calcium; the sulfatic activation by gypsum; and the sulfate-calcium (by a mixture of gypsum and lime) or sulfate-sodium activation (by a mixture of gypsum and sodium) [10]–[12]. In the present study, a calcium activation of the slag with the Portlandite $Ca(OH)_2$ generated during clinker hydration is considered in this study.

Despite the fact that several studies have focused on the hydration processes of slag-blended cement, the effects of the substitution rate of clinker by slag on both hydration kinetics and mechanisms and on microstructural properties are not well understood yet. A relevant description of these aspects is nevertheless crucial for a better understanding of both the durability and mechanical properties of cementitious materials formulated with slag.

The development of a complete hydration model that combines the kinetic and chemical aspects can be considered an interesting tool.

Concerning the prediction of hydration kinetics of slag-based cement, different types of approaches have been proposed in the literature: analytical and numerical ones. For example, Merzouki et al. [13] adopted analytical Knudsen's model [14] initially developed for OPC (see Appendix A), to simulate the hydration kinetic of slag with the purpose of predicting the early age shrinkage of BFS-blended cement. In terms of results obtained, the hydration rates of slag-mixed cement pastes are accurately reproduced for low slag substitutions (less than 30%) but are underestimated for higher amounts of slag.

Concerning numerical models, Kolani et al. [15], [16] simulated the hydration kinetics using the resolution of equations of mass and heat balances which requires calibration parameters based on the Langavant semi-adiabatic calorimeter test. The thermodynamic calculations, using the geochemical code PHREEQC proposed by Elakneswaran et al. [17] for BFS-based cement involved the hydration rate of individual clinker minerals as described by Parrot and Killoh [18] while the hydration kinetic of slag was analytically expressed as a function of time, slag replacement, and activation energy respectively (see Appendix A). However, according to the authors themselves, the derived equation needs to be assessed for a high replacement of cement by slag because it was obtained for replacement levels of up to 60% slag. The model developed by Wang et al. [19], [20], and adopted by Seung and Wang [21], is based on numerical integration of differential equations related to the hydration rates of clinker and slag respectively (Appendix A). The hydration of clinker accounted for a period of initial dormancy, a process of phase-boundary reaction, and a process of diffusion while that of slag considered the consumption of Portlandite formed during the hydration of clinker. The calibration of the model parameters was determined based on isothermal calorimetry measurements for concrete mix formulated with 40% clinker replacement by slag, and then it was tested and validated on two formulations containing 42% and 67% of BFS until one year. The predicted results of the slag hydration degree obtained until one year on two formulations containing 42% and 67% of BFS were overestimated compared to experimental ones. Recently, Park et al. [22] also adopted the kinetic hydration model suggested by Wang et al. [19], [20] as well. In their study, they employed the outcomes of the hydration model as input data for a thermodynamic model implemented in GEM-Selektor [23] and aiming to assess the phase composition of slag-based cement during the hydration process. However, the validation of the model was conducted on materials hydrated until 100 days and incorporating up to

50% BFS.

Concerning the description of chemical reactions, a relevant stoichiometric model has been developed by Chen and Brouwers [24] even though it does not take into account the evolution of hydration limiting its application to well-hydrated materials. Similar stoichiometric approaches have also been adopted by Kolani et al. [15], [16] and by Königsberger and Carette [25]. However, Kolani et al. have predicted the hydration kinetics in addition to chemical reactions as mentioned above, while Königsberger and Carette estimated the evolution of the hydration degree of slag-based calorimetry measurements.

Finally, several multi-components hydration and microstructure models based on geochemical approaches also exist and use discretization, vector, or cellular-automata approaches to depict cement particles as circles, spheres, or discretized components, such as the Jennings and Johnson model [26], Navi and Pignat [27], HYMOSTRUC [28], HydratiCA [29], μic [30], CemGEMS [31], and CEMHYD3D [32] and VCCTL [33]. The benchmark of slag hydration models presented by Atallah et al. [34] concluded that analytical models appear to provide reliable results (relatively close values of porosity, Portlandite, CSH, CASH, and other hydration products) in a short computational time.

The correlation of the mechanical behavior and the hydration properties of slag-based cement has been widely studied in the literature. De Schutter and Taerwe [35] proposed an analytical expression involving formulation parameters (cement composition, water-cement ratio, aggregate properties, and curing conditions) which allows to fit and not to predict the compressive strength evolution over time utilizing calibration parameters. Such an approach has been adopted by other authors [36]. Wang et al. [37] observed a linear correlation between the compressive strength and the mean hydration degree of slag-blended cement. Seung and Wang [21] developed an analytical prediction model of the compressive strength evolution that accounted for the content of CSH and CASH formed by the hydration of clinker and slag respectively. A good agreement is observed between calculated and experimental results obtained on different concrete mixes incorporating slag. A similar type of model has been recently proposed by Wang [20] by considering not the CSH and CASH phases but the hydration degrees of clinker and slag respectively associated with calibration coefficients. Nevertheless, the model was not validated in the long-term.

Elasticity modulus is another important mechanical property, which has to be investigated for cementitious materials formulated with mineral additions. For BFS-blended cement, the evolution of elasticity modulus depends on many parameters, such as the slag used, the curing condition, and the activation method, even if a decrease is reported in many studies (Wang [38], Zemri and Bouiadjra [39], and Khalifa et al. [40]). This change in the elastic modulus is generally related to the properties of the hydrates formed during the hydration of the slag but also to its lower hydration kinetic. Vakhshouri and Nejadi [41] cited in their literature review several existing empirical models that correlate the Young modulus mostly with the compressive strength so that they are not able to take into account directly the hydration properties.

2 Research aims

This study is dedicated to improve knowledge of the long-term hydration, microstructure, and mechanical characteristics of BFS-blended cement through a relevant hydration model in terms of both hydration kinetics and chemical reactions.

The implementation of such hydration model described in section 3 represents the first objective of this work as shown in Figure 1 and is conducted according to the following strategy:

- The prediction of hydration kinetics through analytical models is addressed in section 3.1. The validation of the calculations hypothesis and the calibration of the parameters involved in the models are achieved based on the results of TGA and XRD measurements carried out on four cement paste mixtures formulated with various rates of slag at different ages varying from 7 to

1095 days. Measurements methods are detailed in section 4 while validations are presented in section 5.1.

- The chemical reactions occurring during the hydration process are described in section 3.2 by using a modified version of Kolani et al.'s stoichiometric model [15], [16].

Once implemented, different types of output data as recorded in Figure 1 can be predicted from the hydration model such as amounts of hydrated and anhydrous phases or dry densities. Comparisons with various results from the literature have been made in section 5.2 to validate the approach proposed in the present study. Porous structure evolutions are also investigated in section 5.3 in terms of partition between capillary and CSH gel pores by comparing the capillary porosity predicted by the model with the total porosity measured experimentally.

The second objective of this paper, detailed in section 5.4, concerns the estimation of mechanical properties *i.e.* compressive strength and elasticity modulus respectively, based on the hydration model's output data. The prediction of compressive strength is achieved in section 5.4.1 by using the analytical model adopted by Seung and Wang [21] CSH and CASH content respectively. Finally, correlations between elasticity modulus and predicted hydration degrees of clinker and slag respectively are established and validated in section 5.4.2.

A table of symbols summarizing all the used parameters is provided in Appendix B.

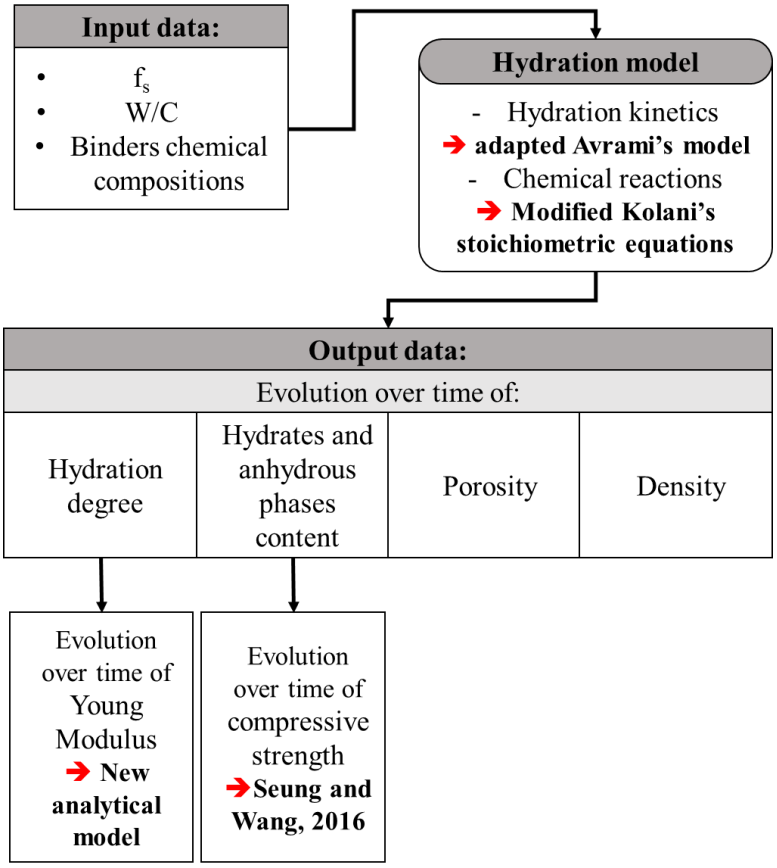

Figure 1: Methodology adopted in the present study

3 Hydration model

3.1 Hydration kinetics

According to [42]–[44], the mean hydration degree of a slag-blended cement is calculated as the weighted average of the hydration degrees of clinker and slag, respectively, in equation (1).

$$\alpha = f_c \times \alpha_c + f_s \times \alpha_s \quad (1)$$

Where f_c(%), and f_s(%) are the clinker and slag content, respectively. From an experimental point of view, different methods are proposed in the literature to estimate the mean hydration degree α, such as Differential Scanning Calorimetry (DSC), X-ray Diffraction (XRD), Scanning Electron Microscopy (SEM), Electrical Conductivity Measurement, and Thermogravimetric Analysis (TGA) [45], Nuclear Magnetic Resonance (NMR) [43]. In the present study, the TGA method described in section 4.2.1 and previously published by Deboucha et al. [44] based on research conducted in our laboratory, is adopted in the present study.

Among the most used hydration kinetic equations of cement-based materials available in the literature, the Avrami exponential-type function [46]–[48] is chosen to predict the hydration degrees of clinker and slag respectively. In fact, as reported by Tennis and Jennings [49], Avrami equations are best suited to describing nucleation and growth reactions.

The expression of the Avrami model is the following (equation 2):

$$\alpha_i = \alpha_{i,max} \times [1-\exp(-S_i \times (t)^{n_i})] \quad (2)$$

Where i represents the clinker or the slag and $\alpha_{i,max}$ corresponds to the ultimate hydration degree of the component i. S_i represents a rate constant that combines the effects of nucleation, multidimensional growth, geometric shape factors, and diffusion of the binder i, while n_i is an exponent that combines the time dependences of the nucleation and growth processes [50]–[53]. Of course, it is expected that the values of these parameters probably vary from one mix formulation to another due to the interdependencies between clinker and slag hydrations that are not considered in equation 1. For that reason, S_i and n_i are assumed to evolve with respect to the percentage of slag used. At first approximation, linear evolutions are adopted in the present study:

$$n_i = a_{ni} \times f_s + b_{ni} \quad (3)$$

$$S_i = a_{Si} \times f_s + b_{Si} \quad (4)$$

The coefficients a_{ni}, b_{ni}, a_{si}, and b_{si} are thus assumed to be constant and do not depend on the type of formulation.

The ultimate hydration of the clinker $\alpha_{c,max}$ is calculated with the following relationship proposed by Waller [54]:

$$\alpha_{c,max} = 1-\exp(-D \times (W/C)) \quad (5)$$

Where D is a parameter related to the curing condition and W/C is the water-to-clinker ratio, respectively. For air-cured materials, a value of 3.3 has been proposed by Waller [54]. However, for the water-cured specimens considered in this work, a value of D equal to 5 seems to be more appropriate due to a more pronounced hydration.

Once the expression of the ultimate hydration degree of the clinker is defined, the values of coefficients a_{nc}, b_{nc}, a_{sc}, and b_{sc} are calibrated by minimizing squared deviations between predicted values of α_c as given in equation 2 and those estimated at different ages from TGA on cement paste formulation without

slag.

Concerning slag hydration, five parameters have to be determined: $\alpha_{s,max}$, a_{ns}, b_{ns}, a_{ss}, and b_{ss} respectively. To the best of our knowledge, the evolution of $\alpha_{s,max}$ with respect to the substitution rate of clinker by slag has not been clearly established in the literature. Hence, a linear evolution is also proposed for Ss and ns at first approximation. We thus obtain the following relationship with two supplementary constant coefficients: $a_{\alpha s}$ and $b_{\alpha s}$ respectively.

$$\alpha_{s,max} = a_{\alpha smax} \times f_s + b_{\alpha smax} \quad (6)$$

All coefficients related to slag hydration kinetic are estimated by minimizing squared deviations between predicted values of α as given in equation 1 and those estimated at different ages from TGA on cement paste mixes formulated with various rates of substitution of clinker by slag. Let us precise that all details about the formulations tested in this study are given in section 4.1.

3.2 Chemical reactions

As mentioned earlier, the stoichiometric calculations developed by Kolani et al. [15], [16], aiming to correlate the chemical composition of the binder with the quantities of their hydration products, are adopted to describe the chemical reactions occurring during the hydration process of slag-blended cement. It is worth reminding that a coupled approach between kinetics and chemical aspects has also been considered by Kolani et al. [15], [16] so that the concentrations of hydrated and anhydrous phases involved in the stoichiometric calculations were expressed as functions of the hydration degree rates of clinker and slag respectively. These latter were determined by the numerical resolution of a system of equations of mass and heat balances. Moreover, Langavant calorimeter results are required as input data.

In the present study, calculations related to kinetics and chemical aspects are decoupled from each other, as done for example by Merzouki et al. [13], to achieve a simplified analytical resolution. For that reason, the concentrations of hydrated and anhydrous phases are directly expressed as a function of time in the stoichiometric calculations proposed by Kolani et al. [15], [16].

During the hydration of a BFS-blended cement, two categories of hydrates can be distinguished:

Those produced by the hydration of clinker, which are respectively

- Calcium silicate hydrates noted as CSH,
- Portlandite $Ca(OH)_2$ noted as CH,
- Ettringite ($C_6A\bar{S}_3H_{32}$) noted as AFt
- Monosulfoaluminate ($C_4A\bar{S}H_{12}$) noted as AFm.

And those produced by the hydration of slag, which are respectively:

- Calcium and aluminum silicate hydrates noted as CASH
- Hydrotalcite (M_5AH_{13}) noted as HT
- Ettringite noted as Aft_s
- Hydrogarnet noted as AH

The molar mass and molar volume of the different hydrates considered in this study are represented in Appendix C.

Once the hydration degrees are known, the mass of the hydrated and non-hydrated phases can be determined following the equations:

$$m_{i,hydrated} = \alpha_i \times m_{i0} \quad (7)$$

$$m_{i,non\text{-}hydrated} = (1-\alpha_i) \times m_{i0} \quad (8)$$

Where $m_{i,0}$ represents the initial mass introduced in the mixture for each component i (clinker or slag).

Depending on the chemical composition of cement and slag, the amounts of hydrated oxides are calculated using the following equation:

$$[j]_{hydrated,i} = m_{i,hydrated} \times F_{j,i} / M_j \quad (9)$$

Where j represents the different oxides in the anhydrous phases.

$[j]_{hydrated,i}$ is the molar concentration (mol/g) of the hydrated oxide j in the initial introduced mass of component m_{i0}; $F_{j,i,}$ and M_j represent the percentage of the oxide j in the binder i, and the molar mass of j (g/mol), respectively. The stoichiometric tables are detailed in Kolani's thesis [16].

Based on the calculation hypothesis adopted by Kolani [15], [16], the evolutions with time of the concentration of hydrates formed from clinker hydration only are calculated as follows:

1) CSH:

$$[CSH]_{c,\ formed}(t) = [S]_c(t) \quad (10)$$

2) Portlandite :

$$[CH]_{c,\ formed}(t) = [C]_c(t) - (C/S)_c \times [S]_c(t) - [\dot{S}]_c(t) - 3 \times [A]_c(t) \quad (11)$$

Where $(C/S)_c$ represents the molar ratio (calcium to silicate content) in CSH. A value of $(C/S)_c$ equal to 1.7 is chosen in this study based on findings by Richardson [55] and reported in several works. The water demand of the CSH $(H/S)_c$ is suggested by Brouwers [56], and it is equal to $((C/S)_c + 0.8)$.

The hydration of clinker results in the formation of an initial quantity of Portlandite noted as $[CH]_{c,\ formed}$. The activation of BFS requires the consumption of an amount of the existing Portlandite, resulting in a remaining concentration noted as $[CH]_{c,\ remaining}$ has to be defined.

A simplified assumption has been made in the present study concerning the estimation of $[CH]_{c,\ remaining}$ that is considered to be proportional to the $[CH]_{c,\ formed}$ (equation 11). Let us specify that in the original model developed by Kolani, the remaining amount of Portlandite is calculated by considering the calcium demand of slag reactions, which depends on the hydration degrees of clinker and slag.

The coefficient of proportionality λ, is estimated from the comparison of available CH at different hydration ages from TGA on cement paste mixes considered in this study (see section 5.2.2) and those estimated from the model (Figure 6). A value of λ equal to 0.8 is found. Let us note that a lower value of λ is expected since only 20% of portlandite generated by clinker hydration will be consumed by slag hydration. Such result can be explained by the fact that the amount of CH formed during the clinker hydration may be underestimated by equation (11) for binary cement. In equation (11), the amount of CH formed during the clinker hydration depends only on the chemical composition of the clinker. The influence of the presence of slag is accounted only through consideration of the substitution rate, although interactions between clinker and slag are known to be more complex. A better understanding of such interactions will be investigated in a further study in order to propose a more relevant value of λ.

$$[CH]_{c,\ remaining}(t) = \lambda \times [CH]_{c,\ formed}(t) \quad (12)$$

3) Ettringite and Monosulfoaluminates:

Depending on the amount of sulfate present in anhydrous phases, Kolani et al. [15], [16] proposed two possible cases of reaction concerning the estimation of the amount of ettringite and monosulfoaluminate as follows:

Case 1:

$$[Aft]_{c,\,formed}(t) = 0.5\times[\dot{S}]_c(t) - 0.5 \times [A]_c(t) \quad (13)$$

$$[Afm]_{c,\,formed}(t) = 1.5\times[A]_c(t) - 0.5 \times [\dot{S}]_c(t) \quad (14)$$

If $[Aft]_c(t)$ and $[Afm]_c(t)$ are positive, then they will be considered as hydrates, otherwise, a formation of Hexahydrates (HEXA) and monosulfoaluminate will be considered (Case 2).

Case 2:

$$[HEXA]_{c,\,formed}(t) = [A]_c(t) - [\dot{S}]_c(t) \quad (15)$$

$$[Afm]_{c,\,formed}(t) = [\dot{S}]_c(t) \quad (16)$$

The evolution with time of slag hydrates is calculated as follows:

$$[CASH]_{s,\,formed}(t) = [S]_s(t) \quad (17)$$

$$[HT]_{s,\,formed}(t) = (1/5)\times[M]_s(t) \quad (18)$$

$$[Aft]_{s,\,formed}(t) = (1/3)\times[\dot{S}]_s(t) \quad (19)$$

$$[AH]_{s,\,formed}(t) = [A]_s(t) - (A/S)_{sc}(t)\times[S]_s(t) - (1/5)\times[M]_s(t) - (1/3)\times[\dot{S}]_s(t) \quad (20)$$

Where $(A/S)_{sc}$ represents the molar ratio A/S formed by the slag in the presence of clinker. It is estimated by Richardson [55] by the following relationship:

$$(A/S)_{sc} = (1/4.732)\times[1 - 0.4277*(C/S)_s] \quad (21)$$

Richardson and Groves [57] demonstrated that increasing the BFS ratio in the mixture leads to a decrease in the molar ratio of C/S. It was determined that the C/S ratio for pure slag is 1.14.

In addition, Adenot [58] and Brouwers [56], suggest connecting the water requirements (H/S) of C-S-H with their stoichiometry using the C/S ratio. In this regard, referring to Kolani et al. [15], the following relation is considered: $(C/S)_s = (H/S)_s = 1.14$.

$(H/S)_s$ is the water demand of the CASH of the slag alone. The knowledge of this parameter allows quantifying the reacted water with the CASH. The quantification of the reacted water with all the hydrates leads to the identification of the free water quantity available at each time, allowing further prediction of the porosity.

In the case of BFS-blended cement, the water demand of CASH formed by the hydration of the slag in the presence of the OPC is evaluated by a linear interpolation between the water demand of CSH_c of the OPC and that of $CASH_s$ of the BFS.

$$(H/S)_{sc}(t) = (C/S)_{sc}(t) + 1.45\times((C/S)_{sc}(t) - (H/S)_s(t)) \quad (22)$$

Where the $(C/S)_{sc}$ takes into consideration both hydrates, CSH and CASH, as follows:

$$(C/S)_{sc}(t) = (C/S)_c\times k_c(t) + (C/S)_s\times k_s(t) \quad (23)$$

It is important to clarify that the formation of the CASH requires the presence of a source of calcium. In the studied formulation, the two sources are the $[CH]_{c,\,remaining}$, and $[C]_{hydrated,s}$. It is worth noting that Kolani [15], [16] considered these two equations related directly to the remaining quantity of Portlandite and calcium oxide in the slag. However, as the proportions of Portlandite and calcium in hydrated slag are simply identified with time in this study, k_c and k_s are proposed to satisfy the calcium demand of slag hydrates, to consume the necessary calcium, in proportion to the quantities available in each source

as follows:

$$k_c(t) = [[CH]_{consumed}(t)] / [(([CH]_{consumed}(t)) + [C]_{hydrated,s}(t)] \quad (24)$$

$$k_s(t) = [C]_{hydrated,s}(t) / ([CH]_{consumed}(t) + [C]_{hydrated,s}(t)) \quad (25)$$

Finally, the mass and volume of the hydrates are calculated by multiplying the molar content by either the molar mass or the molar volume, respectively, as shown in the following equations:

$$m_{h,i}(t) = M_h \times [h]_i(t) \quad (26)$$

$$V_{h,i}(t) = V_{m,h} \times [h]_i(t) \quad (27)$$

Where h, $[h]_i$, M_h, and $V_{m,h}$ are the hydrates, the content of this hydrate h in component i, the molar mass and the molar volume of the hydrate h respectively.

The evolution of the remaining Portlandite with respect to the solid mass available at time t is also taken into consideration, to be compared at a later stage to the results of the TGA measurements. In order to estimate it, the following equation is proposed:

$$\%_m\, CH_{remaining}(t) = m\, CH_{remaining}(t) / [\sum(m_{i,hydrated}(t) + m_{i,non\text{-}hydrated}(t) - m(rw)_i(t))] \quad (28)$$

Where $m_{rw,i}$ represents the mass of the reacted water of each hydrate of the binder i at time t. It can be calculated from the quantity of the reacted water in moles per mole of hydrate "$n(rw)_h$" in each binder, which can be identified from the chemical formula of the hydrate. These quantities are represented in Table 1 for each hydrate.

h_i	CH_c	CSH_c	Afm_c	Aft_c	$(C_3AH_6)_c$	Ah_s	HT_s	Aft_s	CASH
$n(rw)_h$	1	$(H/S)_c$	12	32	6	13	13	32	$(H/S)_{sc}(t)$

Table 1: Water demand of each hydrate

Then the sum of the reacted water at time t can be given as follows:

$$\sum m(rw)_i(t) = n(rw)_h \times [h]_i(t) \times M_{H2O} \quad (29)$$

Where M_{H2O} is the molar mass of water (18 g/mol).

Concerning the dry density, which represents the mass of solid phases corresponding to a given volume, it can also be estimated with the model using the following equation:

$$\rho_{dry}(t) = \sum (m_{h,i}(t) + m_{i,non\text{-}hydrated}(t)) / (V_{total}) \quad (30)$$

For the estimation of the capillary porosity, the calculation of the capillary pores volume is required and given in the following equation:

$$V_{cap\ pores} = \sum (V_{i0} + V_{entrapped\ air}) - (V_{h,i}(t) + V_{i,non\text{-}hydrated}(t)) \quad (31)$$

Where V_{i0}, $V_{i,non\text{-}hydrated}$, and $V_{entrapped\ air}$ are the initially introduced volume, the volume of the non-hydrated phases of the binder i, and the volume of the entrapped air, respectively.

$$V_{i0} = m_{i0} / \rho_i \quad (32)$$

$$V_{i,non\text{-}hydrated}(t) = m_{i,non\text{-}hydrated}(t) / \rho_i \quad (33)$$

$V_{entrapped\ air}$ is measured experimentally and is found to vary around 3.57% of the initially introduced volume V_{i0}.

The capillary porosity can then be written as follows:

$$\Phi_{cap}(t) = V_{cap\ pores} / (V_{i0} + V_{entrapped\ air}) \quad (34)$$

4 Experimental procedure and characterization methods

This experimental campaign is established by studying slag-based cement pastes formulated with four different substitution rates (by mass) of clinker by BFS, *i.e.*, 0%, 30%, 50%, and 80%, respectively, and labeled as P0, P30, P50, and P80. A constant value of water-to-binder ratio equal to 0.5 is chosen for all formulations, allowing comparison of the results with a normalized mortar in a further study.

4.1 Materials

The clinker used is CEM I 52.5 N SR5 PM-CP2 HTS cement produced by Lafarge. The BFS is produced by Ecocem in Dunkerque, France. The physical and chemical properties of OPC and BFS are shown in Table 2 and Table 3, respectively. BFS is obtained by quenching the slag in water at the outlet of the Dunkerque blast furnaces using a new-generation granulator (INBA®). Tap water is used for the preparation of mixtures.

Property	OPC	BFS
Specific gravity (g/cm^3)	3.17	2.9
Specific surface area (cm^2/g)	3635	4450
Loss of ignition (950°C)	1.4	< 1.5%
Passing at 32 µm	--	≥ 0.5%

Table 2: Physical properties of OPC and BFS

% of components	OPC	BFS
SiO_2	23.2	34.9
Al_2O_3	3.1	10.9
Fe_2O_3	2.24	0.5
CaO	66.4	42.3
MgO	0.76	6.9
SO_3	2.22	0.1
K_2O	0.18	0.45
Na_2O	0.11	0.35
TiO_2	0.15	0.7

Table 3: Chemical compounds of the OPC and BFS

The four cement paste mixtures were cast into 40*40*160 mm^3 molds according to the NF EN 196-3 standard [60]. After casting, plastic films were placed over the molds for 24 hours to reduce water evaporation. Following the demolding process, the samples were immersed in water to achieve saturation, hence enhancing the hydration reactions.

4.2 Microstructure identification

4.2.1 ThermoGravimetric Analysis (TGA)

TGA is necessary for the first calibration and then the validation of the hydration model in terms of

hydration kinetics and in terms of the quantification of hydrates formed. TGA is conducted on ground powder having a particle size lower than 0.4 µm in a nitrogen atmosphere. The apparatus used is a TG/DSC-1, STARe Software 9.30, Mettler-Toledo, with a balanced accuracy of 0.1 µg. All the samples are decomposed during a dynamic heating ramp ranging between 20 and 1025 °C at a rate of 5°C/min. The powder was not dried prior to TG tests to avoid hydrate instability [44], [59], [61].

The decomposition of cement hydrates is observed during TGA by decreased endothermic peaks on the derivative TGA. In general, cement hydrate decomposition may be divided into three stages:

- between 25 and 400 °C:
  - Removal of the evaporable water (25 to 105°C)
  - dehydration reaction of CSH and CASH noted as "Ld_h" (105 to 400 °C)
- between 400 and 600 °C: dehydroxylation of Portlandite, noted as "Ld_x"
- between 600 and 800 °C: decarbonation of $CaCO_3$, noted as "Ld_c"

The temperature ranges as well as the TG results of the P0 and P80 at 360 days are presented in Figure 2 in order to visualize the differences obtained between these two formulations. Furthermore, the temperature ranges of each phase vary from one author to another, with low differences depending on the machine used [44], [62], [63].

Based on TG results, a method developed by Monteagudo et al. [62] and recently improved by Deboucha et al. [44] is used to estimate the mean value of hydration degree (see Figure 2). Such a method is based on a measurement of the chemically bound water of mineral additions blended into cement paste at time t "$W_B(t)$" with respect to the ultimate chemically bound water ($W_{B\infty}$) and mass of equivalent binder (L_{eq}) in the sample as described in equation (35).

$$\alpha = (W_B(t)) / (W_{B\infty} \times L_{eq}) \quad (35)$$

$W_{B\infty}$ (g) is considered equal to 0.24, as assumed by several authors [44], [62]. The mass of equivalent binder L_{eq} (g) is calculated as equation (36) by introducing the activity coefficient K = 0.9 for the studied slag according to EN NF 206-1 and NF P18-305 standards [64], [65].

$$L_{eq} = m_c + K \times m_s \quad (36)$$

The calculation methods for m_C and m_S are given in equations (37) and (38).

$$m_C = [m_{sample} - m_B \times (f_S + W/B)] / [(1 + LOI_C)] \quad (37)$$

$$m_S = [m_{sample} - m_B \times ((1 - f_S) + W/B))] / [(1 + LOI_S)] \quad (38)$$

Where m_B, fs, W/B, and LOI represent: the binder mass (g), the replacement rate of OPC by slag, the water/binder ratio, and the loss on ignition, respectively. W_B can be calculated as follows:

$$W_B(t) = Ld_h + Ld_x + 0.41(Ld_c - Ldc_S) - (m_C \times LOI_{CC} + m_S \times LOI_{SC}) + m_d \quad (39)$$

Where Ldc_S, LOI_{ic}, and m_d are the relative mass losses during the decarbonation phase (between 600 and 1000 °C) of the anhydrous material, the loss on ignition of anhydrous powder mass, and the device's drift, which is the mass variation of an empty crucible (g) subjected to a high temperature, respectively. The constant "0.41" represents the conversion factor, which allows assuming the bound water is derived from carbonated Portlandite [44].

The determination of the experimental content of Portlandite at a given period of time t with respect to the dry mass is also possible. It is given by following the equation, based on TGA:

$$\%Ca(OH)_2(t) = (Ld_x \times M_{Ca(OH)2}) / (m_{600°C} \times M_{H2O}) \quad (40)$$

The calculation details of the mean value of the hydration degree are recorded in Appendix D; moreover,

the output data of the TG are published in the dataset [66] as supplementary materials.

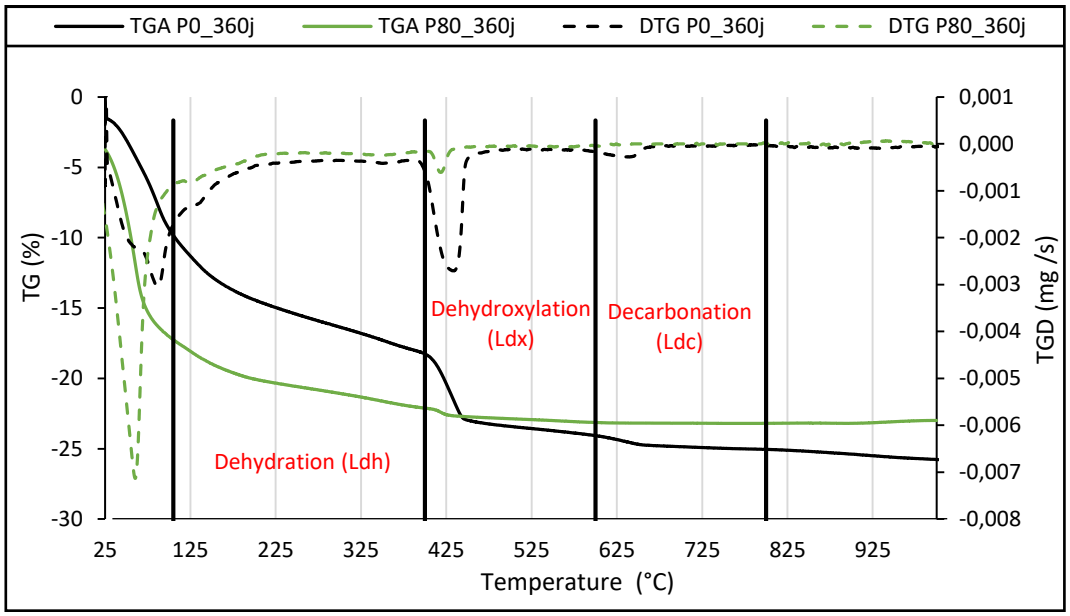

Figure 2: TG and DTG for all the formulations at 360 days

4.2.2 X-ray diffraction (XRD)

XRD analysis was performed to confirm the nature of the crystallized hydrates formed that are considered in the stoichiometric calculations and also to validate the tendency provided by the model regarding the evolution of their concentration. Tests are carried out on cement paste powders obtained after grinding and sieving through a 40-µm sieve. During the preparation phase, hydration was stopped using acetone [67]. Measurements were performed using a SEIFERT Calypso X-ray diffractometer with Co Kα radiation and a constant scanning speed of 0.05° per 5 seconds in the range 2θ = 4°-140°. The results presented in this work are varying between 2θ = 5°- 65°. An acceleration voltage of 40 kV and a current of 40 mA are applied as analysis conditions.

4.2.3 Porosity

Water Porosity

Studying the water porosity of cementitious materials has a significant interest due to its importance in understanding and optimizing the performance of the materials as well as the effect of the BFS on this property.

The water porosity is measured according to the procedure described in the French standard NF P 18 – 459 [68]. It is calculated as follows:

$$\Phi = (m_{sat}-m_{dry})/(m_{sat}-m_{hydro}) \quad (41)$$

Where Φ, m_{sat}, m_{dry}, and m_{hydro} are the porosity, the saturated mass of the sample, the dry mass measured after drying at 105 °C, and the hydrostatic mass, respectively.

Dry density

The measurement of the dry density is taken on the same samples used to measure the water porosity at 105°C. The calculation of the dry density is measured following the equation:

$$\rho_{dry} = (m_{dry})/(m_{sat}-m_{hydro}) \quad (42)$$

4.3 Mechanical properties

4.3.1 Compressive strength

The compressive strength was measured according to the NF EN 196-1 standard [69] by using a testing machine of 250 KN capacity. The results obtained are the average, minimum, and maximum values of six measurements.

4.3.2 Young Modulus

The measured values of the Young Modulus are based on the vibration frequencies, which are measured using a GrindoSonic® brand quick fundamental frequency analyzer. The measurement instrument includes a piezoelectric transducer with a metal tip that can collect vibration frequencies ranging from 20 to 100 kHz at one place on the specimen. The modulus is then calculated using equation (43):

$$E=0.9465\times(m\times f_f^2/b)\times(L^3/t^3)\times T_1 \quad (43)$$

Where E, f_f, L, b, and t denote Young's modulus (Pa), flexural frequency (Hz), mass in (g), length in (mm), and width in (mm). T_1 is a correction factor that compensates for the bar's finite thickness, Poisson's ratio, and other factors. Flexible and absorbent foam is placed under the prism to limit the interference of the specimen's vibration with the table.

The resulting frequency values are then recorded to calculate Young's modulus according to the standard NF EN ISO 12680-1 [70]. The presented values are the average ones and are presented with their standard deviation.

5 Results and discussion

5.1 Hydration kinetics

In general, the hydration kinetic of BFS is much slower than that of OPC. Figure 3 shows the hydration kinetics for the four cement paste formulations considered in the present study. After 7 days, hydration degrees of 0.67, 0.54, 0.53, and 0.38 are obtained for P0, P30, P50, and P80, respectively. These results are consistent with the dilution effect played by slag in the short term as reported in [66].

Despite an increase in hydration degree values between 7 and 360 days (0.91, 0.83, 0.73, and 0.49 for P0, P30, P50, and P80, respectively) at 360 days. The dilution effect of slag seems predominant yet, even though its hydration has probably started, as confirmed by the stabilization of the amount of Portlandite (Figure 6), meaning that the ratio between the consumption and formation of Portlandite seems to be constant.

At 530 days, the hydration degrees of the slag-blended cement pastes, especially P30, significantly increase and become comparable to that of P0. The hydration degrees became 0.87, 0.89, 0.76, and 0.62 for P0, P30, P50, and P80, respectively. After this point, all the hydration degrees measured for P0 and P30 maintain very close values, while the hydration degrees of the two other formulations remain lower.

After 960 days of wet curing, the hydration degrees for P0, P50, and P80, were 0.92, 0.90, 0.73, and 0.53, respectively. The decrease reported between 530 and 960 days for P80 can be related to the uncertainty of the measurement. However, in reality, it seems towards stabilization.

In terms of hydration kinetics, Figure 3 shows that the hydration degree of P0 increases until a value of 0.86 at 90 days, and it continues increasing slowly until a value of 0.9 at 180 days before stabilizing.

Nevertheless, the hydration degrees of slag-blended cement show a sharp increase until almost 90 days. This increasing slope becomes less steep after 90 days, indicating that the hydration continues at a lower rate until 960 days. In other words, after 90 days, the kinetics of hydration of P0 become slower than those of P30, P50, and P80, highlighting that the hydration of slag becomes more pronounced [71]. After this description of the evolution of experimentally measured hydration degrees through the TGA, calibrating the parameters related to the hydration kinetics of clinker and slag as given in equations (2-4) and described in section 3.1, is now possible.

For clinker, the values of coefficients a_{nc}, b_{nc}, a_{sc}, and b_{sc} determined from the experimental results of P0 formulation are reported in Table 4. It is worth noting that applying equations (3-5) in equation (2) results in an increase of α_c by increasing the slag content due to the decrease in the clinker ratio. This may contradict the findings of research [13], [21] concluding that the presence of slag does not influence the clinker hydration since it is regarded as independent of the BFS. However, it is consistent with the previously described dilution effect, which leads to more accessible water for clinker particle hydration as BFS concentration increases [72]. As reported, the experimental results of P0 are used to calibrate the parameters (n_c, S_c, and $\alpha_{c,max}$), however, those of P30, P50, and P80 are used to calibrate the three missing parameters in equation (2) (n_S, S_S, and $\alpha_{s,max}$).

For slag, the coefficients a_{ns}, b_{ns}, a_{ss}, b_{ss}, $a_{\alpha s}$ and $b_{\alpha s}$ are calibrated from the experimental results of P30, P50, and P80 respectively. The obtained values are also recorded in Table 4. As seen, the coefficients vary significantly depending on the slag content; however, it is difficult to physically explain these variations since these coefficients integrate different physicochemical mechanisms.

	Condition	Coefficient related to hydration kinetic	Value
Clinker	always	a_{nc}	-0.078
		b_{nc}	0.370
		a_{Sc}	-0.038
		b_{Sc}	0.620
Slag	always	$a_{\alpha s,max}$	-0.626
		$b_{\alpha s,max}$	1.057
	$f_s \leq 30\%$	a_{ns}	-1.200
		b_{ns}	1
		a_{Ss}	0
		b_{Ss}	0.060
	$30\% < f_s \leq 50\%$	a_{ns}	-1.750
		b_{ns}	1.165
		a_{Ss}	0.697
		b_{Ss}	-0.150
	$50\% < f_s$	a_{ns}	-0.100
		b_{ns}	0.340
		a_{Ss}	0.697
		b_{Ss}	-0.150

Table 4: Calibration parameters

It can be observed that the increase in BFS content leads to a linear decrease of $\alpha_{s,max}$ that can be justified by the reduction in CH as reported in [40], [73].

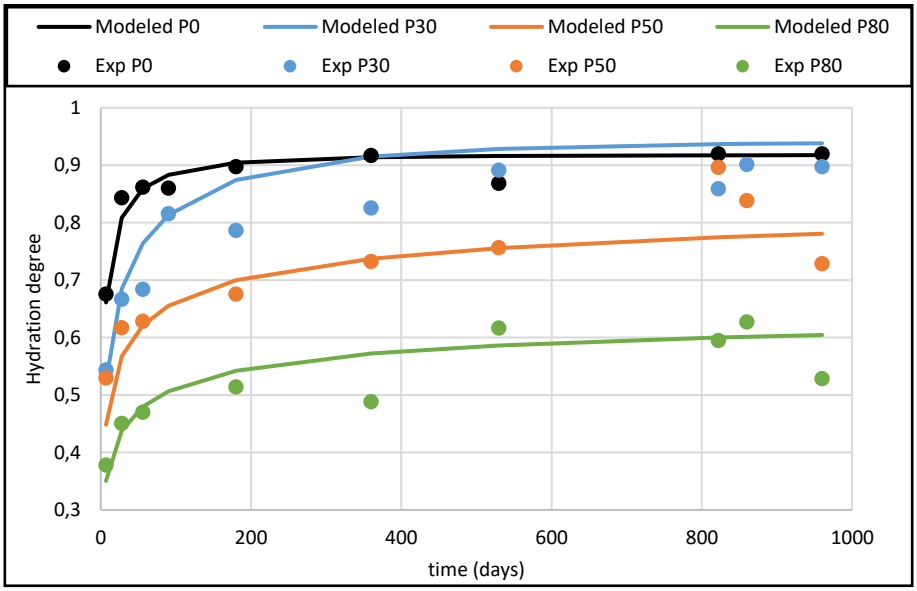

Figure 3: Evolution of the experimental hydration degrees (model calibration)

In order to validate the hydration kinetic models proposed in this study, a comparison between experimental data reported from the literature and the predicted ones was made and presented in Figure 4. The various tested mixes in terms of W/B ratio, curing type and duration, binder compositions, and BFS content, are recorded in Table 5.

Reference	W/B	Cure time	Cure type	BFS content
Stephant [43]	between 0.41 and 0.43	1; 3; 7; 28; 180; 360; 730 days	Water	0%; 14.26%; 61.41%; 80.56%
Darquennes [36]	0.45	0.5; 2; 5; 21; 42; 215; 420; 1970; 4090 days	Air	0%; 42%
Deboucha [44]	0.35	7; 28; 90 days	Air	0%; 20%; 30%; 40%

Table 5: Parameters used in the literature

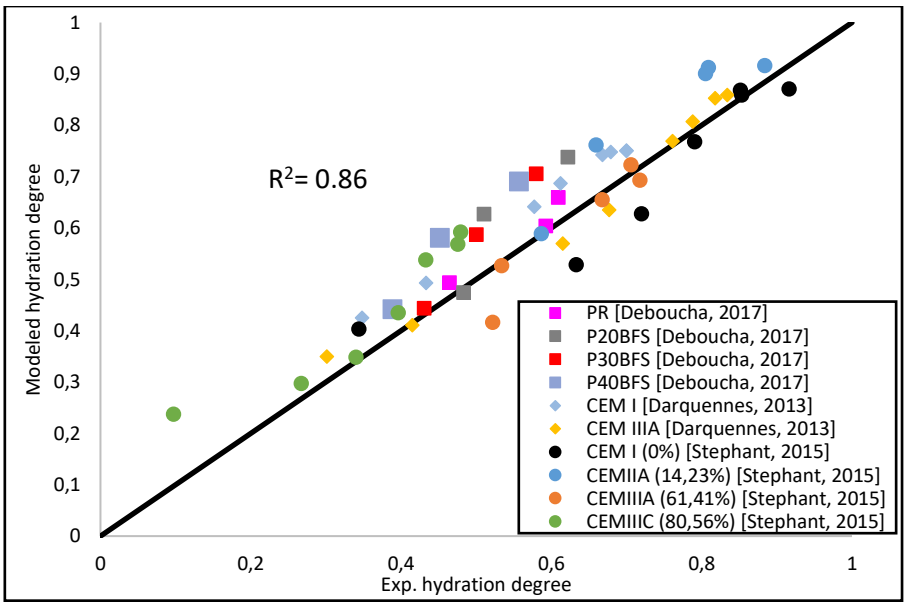

Figure 4: Validation of the hydration kinetics model with the literature ([43], [36], [44])

5.2 Chemical reactions

5.2.1 Hydrates formed using XRD

The formation of specific hydrated phases associated with the hydration of slag and involved in the hydration model, *i.e.*, Hydrotalcite, Ettringite as well as the Portlandite is highlighted in diffractograms shown in Figure 5. As expected, CASH phases are not detected since they are poorly crystallized.

However, small peaks of the anhydrous phase, dicalcium silicate (C_2S), are detected in the OPC until 90 days, as well as very small peaks of Calcite that may be contributed to the calcination of the powder during the grinding process. These phases are also observed in the BFS-blended cement in addition to the ghelhenite (Gh) "crystallized phase of slag" signifying that a portion of the slag is no longer vitreous and will therefore not react. The vitrification rate of the slag used in this study is higher than 90%.

As observed in Figure 5, the increase in slag ratio decreases the intensity of the Portlandite peaks. This decrease can be directly linked to the lower availability of the clinker to be hydrated in these formulations, which leads to lower production of CH.

In terms of hydrate formation evolutions, Figure 5 confirms that the amount of Portlandite increases for the P0 during the time before stabilizing between 180 and 360 days. Such increase is expected given that no consumption of Portlandite occurs during the hydration of clinker. However, for cement pastes formulated with slag, a progressive decrease of Portlandite peak over time is observed between 7 and 360 days due to the consumption of this later to activate slag hydration as discussed in the following section.

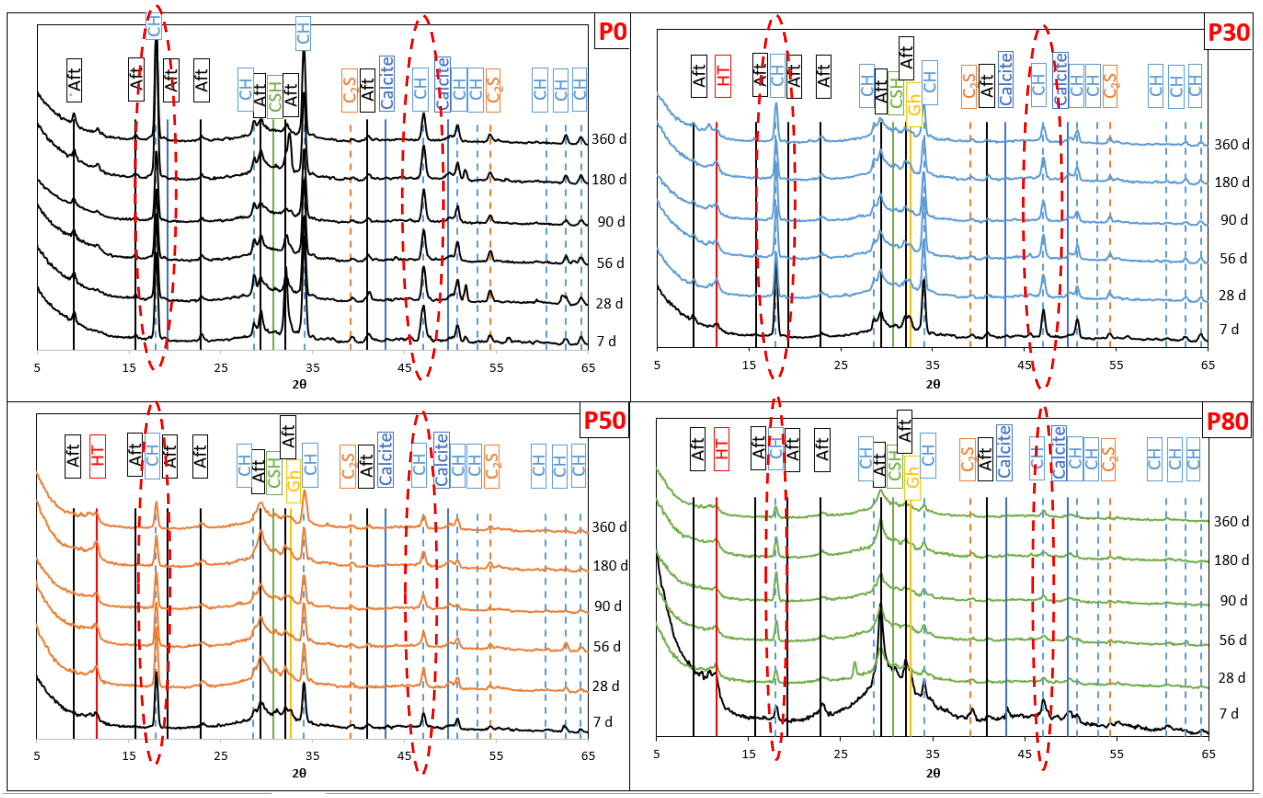

Figure 5: Comparison of diffractograms of different cement pastes between 7 days and 360 days (model validation)

5.2.2 Hydrates content and model's validation

In a first step, the evolution of the Portlandite (CH) is studied, for all the tested cement paste mixes, and

reported in Figure 6. These experimental measurements are calculated using equation (40) based on TGA results, as reported in section 4.2.1.

For P0 formulation, the CH content increases from 23.40% to 25.40% and subsequently to 30.15% at 7, 56, and 90 days, and then seems to be stabilized. In general, a completely hydrated OPC generates around 20 to 25 wt.% $Ca(OH)_2$ [74], [75]. Nevertheless, the weight percentage is measured with respect to the binder mass and not the dry mass. Furthermore, increasing the slag percentage causes a drop in the generated Portlandite caused by the slag dilution effect at early ages. Such drop in CH content is depicted in Figure 5 for P30, P50 et P80 respectively.

The available Portlandite content increases for all the formulations for a certain time (almost 90 days) due to the cement hydration and then stabilizes, which is in agreement with the hydration degree evolution and the XRD analysis. The stabilization over time of the available Portlandite content denotes that the ratio between the Portlandite formed by the hydration of clinker and the remaining ratio after the hydration of slag is almost constant. This seems to be consistent with the proportionality assumption made in this study as given in equation (12). Based on these experimental findings, and based on equations (12 & 28), the coefficient of proportionality λ in equation (12) is calibrated using the evolution of the CH content of the P80 formulation. This coefficient is then validated with CH content of both P30 and P50 formulations but also with CH content from 86 various published results from literature containing between 0 and 80,56% BFS, as shown in Figure 7 and described in Table 5 and Table 6.

However, it is important to note that the proportionality assumption made in equation (12) may not perfectly reproduce the short-term hydration of slag-based cement. In fact, many researchers, such as Wang et al. [19] Königsberger and Carette [25], reported that the CH content in concrete with a higher slag ratio increased first and then decreased at early ages. This observation is not precisely described in the proposed model. Moreover, equation (12) is able to correctly reproduce the overall trend of the Portlandite evolution measured experimentally and reported in the literature, especially in the long-term.

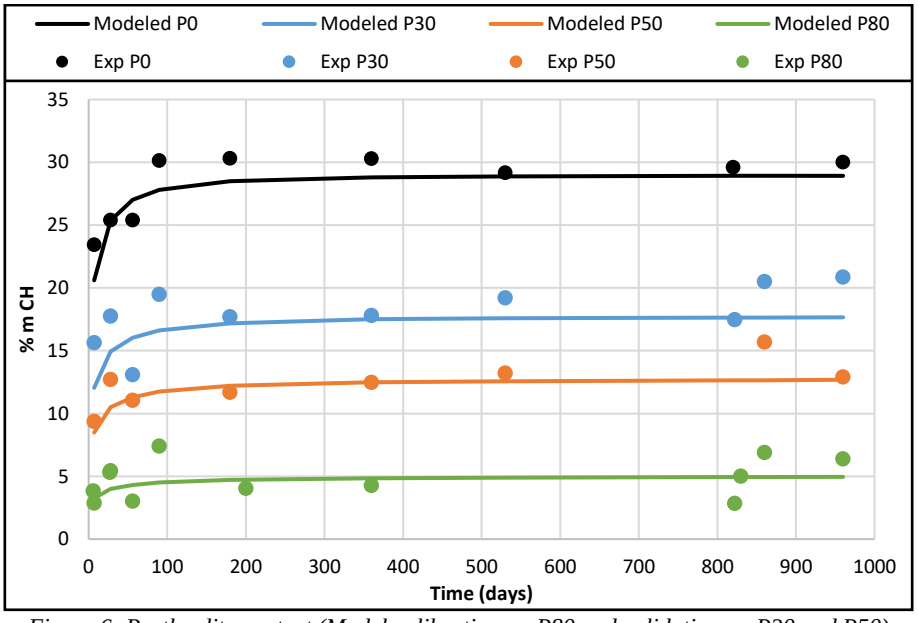

Figure 6: Portlandite content (Model calibration on P80 and validation on P30 and P50)

Reference	W/B	Cure type	BFS content
Merzouki et al. [13]	0.32	Air	0%; 30%; 50%; 80%
Zhao et al. [76]	0.5	Air	50%
Whittaker et al. [77]	0.5	Water	0%; 40%
Kocaba et al. [78]	0.42	Water	40%

Table 6: References issued from literature for CH content validation

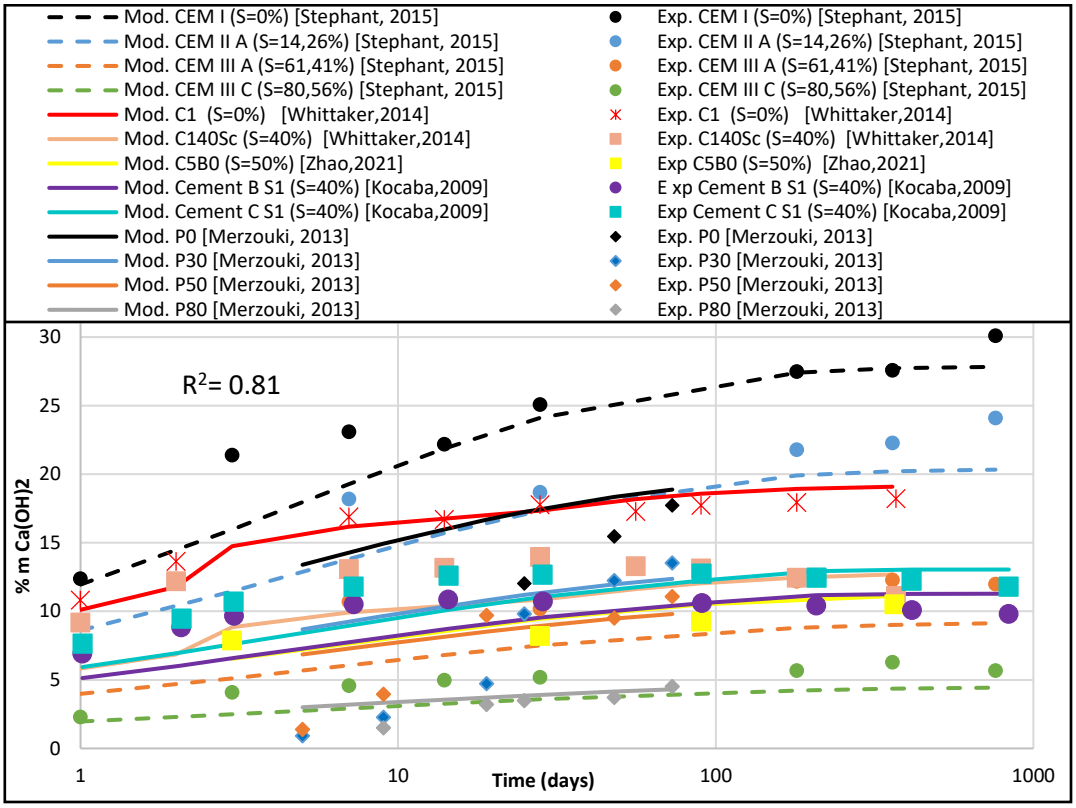

Figure 7: Portlandite content comparison (Literature versus modeled data) (model validation)

In the same context, and to enable the model to predict the quantity of Hydrotalcite, a hydration product relevant to slag, we conduct a validation process. Due to the lack of the necessary materials for quantifying Hydrotalcite content in our laboratory, we validate our model by comparing its predictions with experimental results obtained by Stephant [79] using Nuclear Magnetic Resonance (NMR). This involves determining the aluminum nuclei contribution and assuming that all the magnesium in the cement dissolves to form Hydrotalcite. Nevertheless, Stephant [79] reported that the decomposition of the spectrum is complex so a theoretical error of 10% in the measurement could be related to the deformed ray of the HT due to the lyophilization.

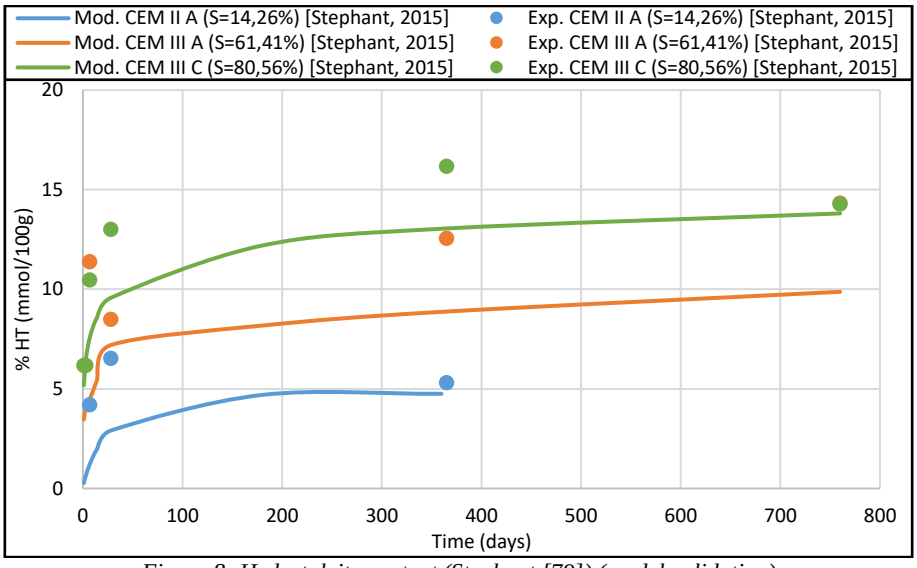

Figure 8: Hydrotalcite content (Stephant [79]) (model validation)

The comparison of experimental and predicted outcomes for different formulations of cement pastes

with varying rates of clinker substitution by slag reveals similar trends, as depicted in Figure 8. The discrepancies observed in Figure 8 can be associated to the theoretical error reported. As expected, the HT content is highly affected by the BFS content. The higher the slag content, the higher the HT fraction.

Finally, given its ability to calculate the amount of both hydrated and anhydrous phases, the hydration model can estimate the dry density as described in equation (30). It is important to highlight that the accurate prediction of dry densities, as demonstrated in Figure 9, serves as an additional method to validate the calculations of anhydrous phases and hydrates, beyond just Portlandite and Hydrotalcite. These include hydrates like CASH or Aft, which might pose challenges when it comes to experimental quantification. Figure 9 highlights that increasing slag content leads to a decrease in dry density due to higher amounts of anhydrous phases. Such result is expected since they are consistent with lower hydration degrees previously shown in Figure 3, leading to higher anhydrous phases.

The dry density of P0 formulation increases significantly until 28 days and then tends to stabilize while a slower but progressive increase is observed for cement pastes formulated with slag. This is attributed to the formation of new hydrates able to fill the existent pores, leading to a decrease in the void ratio and then an enhancement in density, as reported in [80].

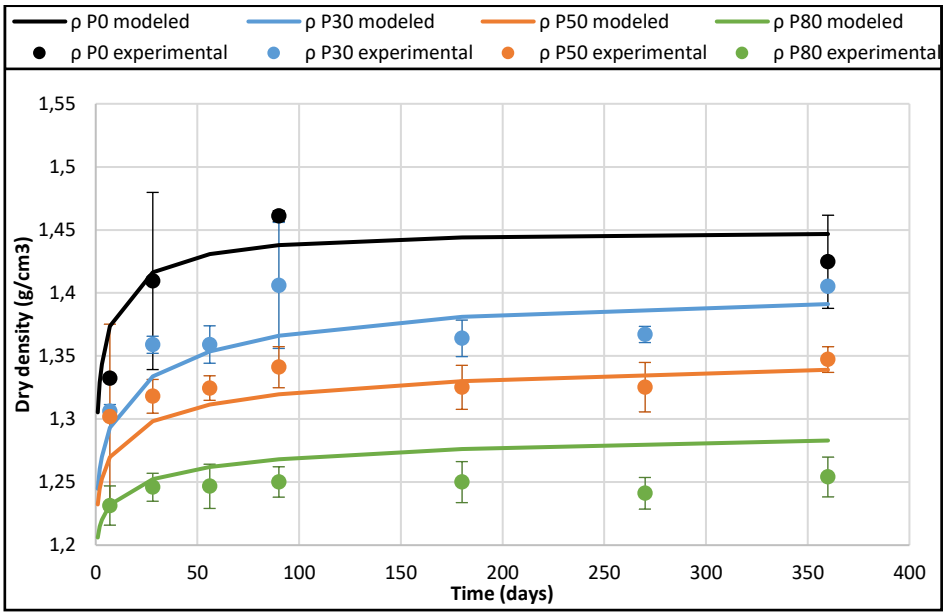

Figure 9: Comparison between experimental and modeled dry density

5.3 Porous structure

The capillary porosity can also be predicted from the hydration as given in equation (34). The initial porosity of the material is related to the volume of mixing water. When the material hydrates, chemical shrinkage occurs and results in the creation of capillary porosity in addition to that induced by residual water not consumed by hydration reactions. Capillary pores, with diameters ranging from a few nanometers to several micrometers, are mainly responsible for fluid transport through the cementitious matrix [81].

However, the effect of slag on the intra-hydrate porosity of CSH and CASH remains a challenge regarding an accurate estimation of the total porosity. Indeed, Chen & Brouwers [24] proposed an estimation of the intra-hydrate porosity with respect to the C/S ratio. For OPC-based materials with a C/S ratio of 1,7, a CSH porosity of around 34%, is found while a lower value of 28% is suggested in other studies [29], [92], and [93]. In addition, the model proposed by Chen & Brouwers and adopted later by Merzouki et al. [13] leads to an increase in intra-hydrate porosity when increasing the

substitution rate of clinker by slag due to the decrease of C/S ratio. This assumption is questioned by a recent study by Königsberger and Carette [25], reporting based on NMR measurements, the formation of a denser CSH gel hydrate in the presence of slag as a consequence of a decrease in its porosity.

Due to contradictory information about the CASH porosity available in the literature, only capillary porosity is considered in the present study. However, a comparison between predicted capillary porosities of slag-based mixes and experimental total ones is proposed hereafter to evaluate the partition of the porosity between capillary and CSH-CASH pores.

A further study will be held to better understand the effect of the slag on the intra-CSH and intra-CASH porosities.

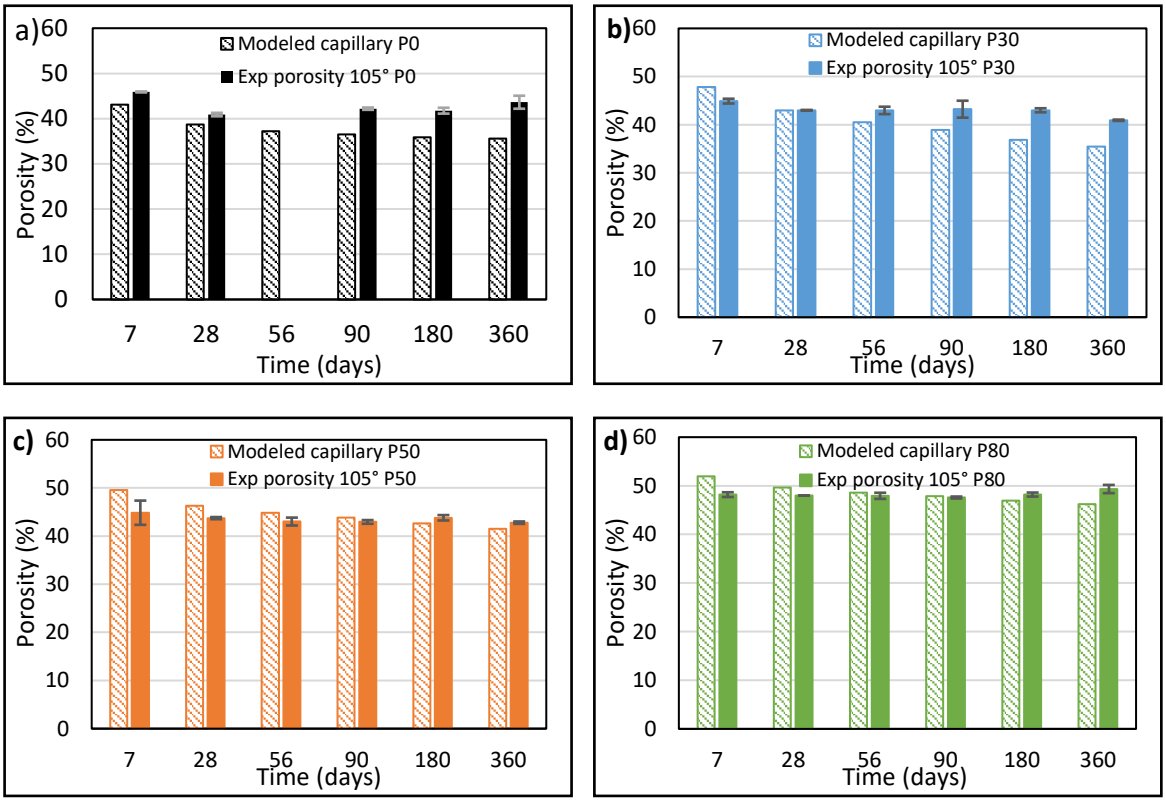

Figure 10: Comparison between modeled capillary and total experimental porosities for a) P0 b) P30 c) P50 and d) P80.

The experimental total porosity decreases with time for all tested formulations. As the hydration proceeds, the formation of hydrates reduces the volume of existing capillary voids.

At 7 days, the total porosity varied from 44.75% to 44.89%, 44.85%, and 48.18% while increasing the percentage of slag from 0% to 30%, 50%, and 80%, respectively.

Compared to the P0 formulation, the P80 mix induces a relatively high porosity. However, comparable porosities were measured until 180 days after adding up to 50% BFS with a maximum variation of 1.1%. It is worth noting that due to a technical problem in the instrument, testing the porosity of P0 at 56 days was not held. According to Figure 10, the total porosity of the different formulations shows varying trends between 7 and 360 days. Specifically, a decrease of 2.26%, 3.98%, and 2.06% for P0, P30, and P50, respectively is obtained. On the other hand, a slight increase of 1.15% is observed for formulation P80, which is likely due to measurement uncertainties. However, by considering the standard deviation of the results for P80 at 360 days, the difference in porosity between 7 and 360 days appears to be negligible.

The important drop in the porosity of P0 and P30 is related to the fact that the hydration degree, in terms of compressive strength and young modulus, of these two formulations seems to reach a maximum value and stabilize as will be presented later on. Nevertheless, the hydration degrees of P50 and P80 continue increasing as reported in Figure 3, which could lead to a decrease in the porosity in later ages.

It is also worth noting in Figure 10 that for P0 and P30 formulations, the gaps between modeled capillary porosities and experimental total ones increase with time while they decrease for P50 and P80 mixes. Such observations would suggest an evolution of CSH-CASH porosity with respect to the substitution rate of clinker by slag and seem to be consistent with the results obtained by Königsberger and Carette [25] even though further investigations are of course necessary to confirm those aspects.

5.4 Mechanical behavior

5.4.1 Compressive strength

The compressive strength (σ_c) of cement paste is an important factor related to the structural integrity of concrete structures. As the hydration process evolves, the cementitious matrix gains strength due to the formation of the CSH and CASH [24], [84]. Figure 11 represents the increase in compressive strength over time for all tested mixes. The compressive strength values are 58 MPa, 44 MPa, 48 MPa, and 36 MPa for P0, P30, P50, and P80, respectively at 56 days. These results are consistent with hydration kinetics and dry density evolutions shown previously. The gap in strength between P0 and slag-based mixtures decreases with time. After 56 days, the strength of P0 tends toward a constant value and reaches 68 MPa after 1095 days. However, the compressive strength values of P30, P50, and P80 keep on increasing progressively due to a continuation of the hydration process.

At 360 days P30 and P50 exhibit identical performance in comparison to that of P0 *i.e.*, around 65MPa while the compressive strength of P80 remains lower with a value of 46 MPa.

At 1095 days, the compressive strength of P30 clearly exceeds that of P0 (75 MPa vs. 68MPa) while performances of P50 and P0 remain comparable. Finally, a gain in strength of 5 MPa is observed for P80 between 360 and 1095 days (51 MPa vs. 46MPa).

Among the existing models that propose a prediction of compressive strength based on a hydration model, the approach developed by Seung and Wang [21] and given by equation (44) can be implemented in the present study since involving the amounts of CSH and CASH. It is however worth noting that Seung and Wang have validated their model slag-based concrete formulations whose hydration ages do not exceed 760 days. The applicability of the model to cement paste formulations hydrated for a longer period than previously is thus tested in this study.

$$\sigma_c(t) = A_1 \times m_{CSHc}(t) / W_0 + A_2 \times m_{CASHs}(t) / W_0 - A_3 \quad (44)$$

Where A_1, A_2, and A_3 are constant strength coefficients equal to 54.31 MPa, 60.51 MPa, and 11.63 MPa, respectively, and are the same as those proposed by Seung and Wang. W_0, m_{CSHc}, and m_{CASHs} are the initial mass of water used in the mix and the mass of CSH and CASH in grams at time t, respectively.

As shown in Figure 11, the modeled compressive strengths are in good agreement with the experimental data, which confirms the validity of the mechanical strength modeling for a slag-based cement paste in the long term (at 1095 days).

Nevertheless, given that Seung and Wang [21], originally proposed the model at a concrete scale and not at a cement paste one, the inclusion of sand and gravel may not have a significant impact on the increase of compressive strength. On the contrary, the presence of aggregates results in a decrease in compressive strength according to Yu et al. [85] and Du et al. [86], due to the existence Interfacial Transition Zone (ITZ).

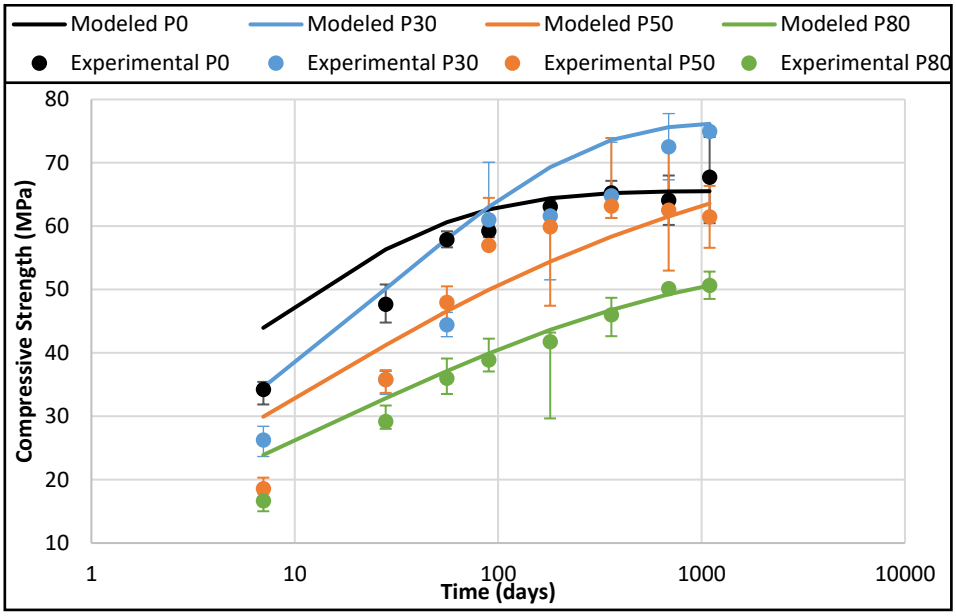

Figure 11: Comparison of the experimental and modeled compressive strength over the curing time (model validation)

Supplementary validations based on cement paste formulations from literature results are proposed in Figure 12. The formulation characteristics are recorded in Table 7. It is worth noting that the measured compressive strengths are carried out at different ages ranging from one to 90 days.

Reference	W/B	Cure type	BFS content
Shaikh and Hosan [87]	0.4	Water / 90 days	60%, 70%, 80%, 90%
Kellouche and Bougara [88]	0.4	Water / 90 days	0%, 50%
Boubekeur et al. [89]	0.5	Water / 90 days	0%, 10%, 20%, 30%, 40%

Table 7: Parameters used in the literature for σ_c validation

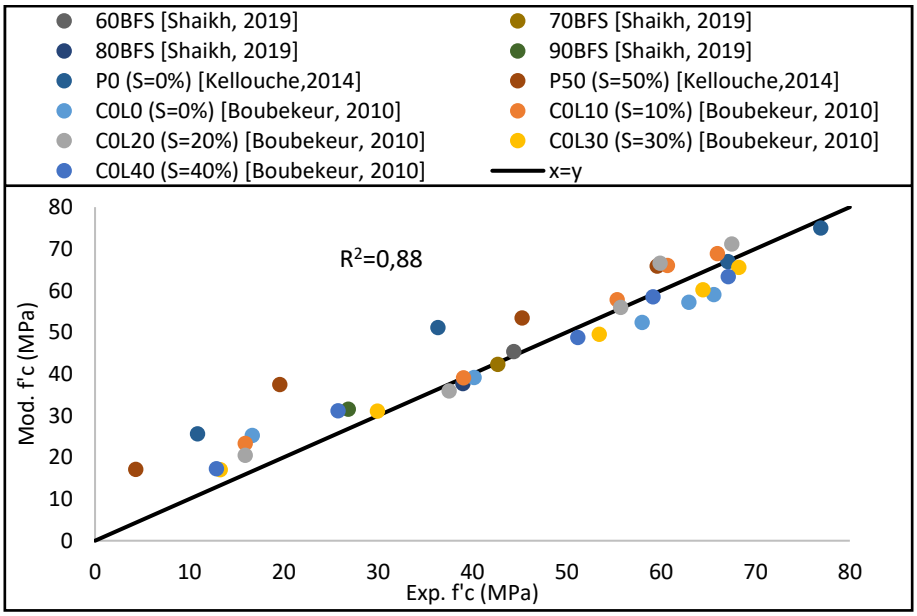

Figure 12: Comparison of experimental and modeled compressive strength for data in literature (model validation)

5.4.2 Young Modulus

The evolution of the amounts of both hydrated and anhydrous phases during the hydration process affects the rigidity of the cementitious matrix. However, not only the CSH and CASH are responsible for the rigidity so that all the hydrates should be considered.

Homogenization techniques could be helpful to achieve a prediction of Young Modulus as performed by Li et al. [90]. However, they cannot be applied to the present study given that the identification of elastic properties of the CSH and CASH with respect to the substitution rate of clinker by slag and to slag activation method among others requires further investigations that are not addressed in this paper. For that reason, only a direct correlation between elasticity modulus and predicted hydration degrees of clinker and slag is proposed in this section.

As reported in the introduction, several empirical models have been proposed in the literature and are mainly correlated with compressive strength but not with hydration characteristics.

Thus, the following relationship between the Young modulus and the hydration degrees of clinker and slag is proposed in the first approximation:

$$E(t) = B_1 \times f_c \times \alpha_c + B_2 \times f_s \times \alpha_s - B_3 \quad (45)$$

Where E is the young modulus in GPa and B_1, B_2, and B_3 are three constants, not age-dependent variables. B1 and B2 are associated with clinker and slag hydration products respectively.

The coefficients B_1 and B_3, respectively equal to 24.4 GPa and 2.4 GPa are determined from the experimental elasticity modulus of P0 formulation while the coefficient B2, equal to 37.8 GPa, is estimated from those of P80 formulation. The values obtained are therefore validated by the good agreement between the predicted elasticity modulus and experimental ones measured on P30 and P50 (Figure 13).

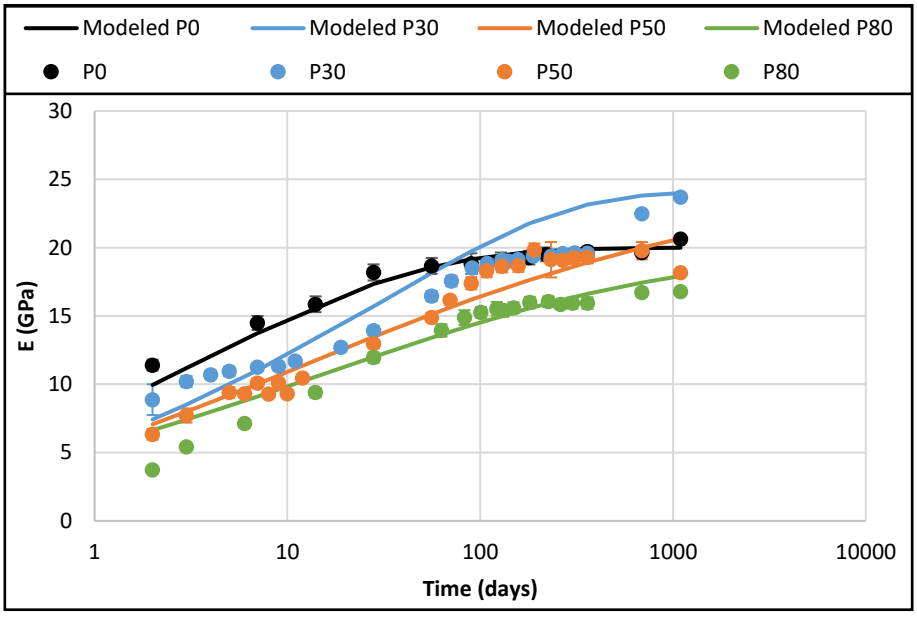

Figure 13: Young modulus evolution (Model calibration on P0, P80 and validation on P30, and P50)

Notably, the young modulus of P0 is significantly higher than that of other formulations incorporating slag, exhibiting a rapid increase until 56 days followed by a more progressive increase until 1095 days. The reduction in the elastic modulus observed with the addition of slag is attributed to the higher concentration of anhydrides, exhibiting lower rigidity compared to hydrates, which is coherent with the

dry density studied in Figure 9. Consequently, this decrease in modulus indicates that this material at the paste scale is more deformable and therefore less sensitive to cracking for example.

However, the inclusion of aggregates can lead to a disparity in rigidity between the matrix and the aggregates, potentially causing issues like differential shrinkage within the sample, which can have adverse effects.

6 Conclusion

In conclusion, this study contributes to a better understanding of the hydration mechanisms in BFS-blended cement through the development of a comprehensive hydration model that incorporates both kinetics and chemical reactions. The main advantage of the proposed approach lies in the fact that it requires a few parameters, which are associated with formulation characteristics such as chemical compositions, water-to-binder ratio, and substitution rate of clinker by slag. These are the main conclusions of this work:

- the hydration kinetics are described using adapted Avrami's exponential models which can take the influence of substitution rate of clinker by slag and the interdependencies of clinker and slag hydration into account.
- the chemical reactions are described using a modified version of Kolani's stoichiometric model to achieve a simplified analytical resolution. The amount of Portlandite consumed by slag hydration is assumed to be proportional to that formed by clinker hydration. The model has been calibrated based on the results of an experimental campaign conducted on four cement paste mixes with different rates of slag varying from 0 to 80% by mass.
- Different output data are well reproduced by the model: Evolutions over time of hydration degree, hydrated phases (Portlandite and Hydrotalcite), and dry densities. Further investigations are nevertheless required to explore the impact of different slag ratios on the porous structure of CSH and CASH, which has not been yet well clarified.

The incorporation of BFS induces a decrease in the the mechanical properties, compressive strength, and Young's modulus before 180 days, however comparable or even higher results are obtained at later stages for the P0, P30, and P50 mixtures.

Additionally, the mechanical properties (σ_c and E) can be well correlated to hydration model results based on existing or new equations, which have to be validated at mortar/concrete scales.

Finally, the prospect of combining the present model with thermodynamic approaches would be interesting to investigate in further studies to achieve a fine description of both the activation of slag hydration and the hydration process itself but also to quantify the risk of early age cracking of concrete structures formulated with slag blended cement.

Acknowledgements

Financial support was provided by « Commissariat à l'énergie atomique et aux énergies alternatives » (CEA-tech).

REFERENCES:

[1] J. Bijen, 'Benefits of slag and fly ash', *Constr. Build. Mater.*, vol. 10, no. 5, pp. 309–314, 1996, doi: https://doi.org/10.1016/0950-0618(95)00014-3.

[2] S. Geetha and S. Madhavan, 'High Performance Concrete with Copper slag for Marine Environment', *Mater. Today Proc.*, vol. 4, no. 2, Part A, pp. 3525–3533, 2017, doi: https://doi.org/10.1016/j.matpr.2017.02.243.

[3] E. Özbay, M. Erdemir, and H. İ. Durmuş, 'Utilization and efficiency of ground granulated blast furnace slag on concrete properties – A review', *Constr. Build. Mater.*, vol. 105, pp. 423–434, 2016, doi: https://doi.org/10.1016/j.conbuildmat.2015.12.153.

[4] A. B. Fraj, S. Bonnet, N. Leklou, and A. Khelidj, 'Investigating the early-age diffusion of chloride ions in hardening slag-blended mortars on the light of their hydration progress', *Constr. Build. Mater.*, vol. 225, pp. 485–495, 2019, doi: https://doi.org/10.1016/j.conbuildmat.2019.07.185.

[5] A. Ben Fraj, S. Bonnet, and A. Khelidj, 'New approach for coupled chloride/moisture transport in non-saturated concrete with and without slag', *Constr. Build. Mater.*, vol. 35, pp. 761–771, 2012.

[6] B. Touil, F. Ghomari, A. Khelidj, S. Bonnet, and O. Amiri, 'Durability assessment of the oldest concrete structure in the Mediterranean coastline: The Ghazaouet harbour', *Mar. Struct.*, vol. 81, p. 103121, Jan. 2022, doi: 10.1016/j.marstruc.2021.103121.

[7] R. Luo, Y. Cai, C. Wang, and X. Huang, 'Study of chloride binding and diffusion in GGBS concrete', *Cem. Concr. Res.*, vol. 33, no. 1, pp. 1–7, 2003.

[8] R. K. Dhir, M. A. K. El-Mohr, and T. D. Dyer, 'Chloride binding in GGBS concrete', *Cem. Concr. Res.*, vol. 26, no. 12, pp. 1767–1773, 1996.

[9] H.-S. Kim, J.-W. Park, Y.-J. An, J.-S. Bae, and C. Han, 'Activation of Ground Granulated Blast Furnace Slag Cement by Calcined Alunite', *Mater. Trans.*, vol. 52, no. 2, pp. 210–218, 2011, doi: 10.2320/matertrans.M2010350.

[10] A. Cheng, R. Huang, J.-K. Wu, and C.-H. Chen, 'Influence of GGBS on durability and corrosion behavior of reinforced concrete', *Mater. Chem. Phys.*, vol. 93, no. 2, pp. 404–411, 2005, doi: https://doi.org/10.1016/j.matchemphys.2005.03.043.

[11] A. Hadj-sadok, S. Kenai, L. Courard, and A. Darimont, 'Microstructure and durability of mortars modified with medium active blast furnace slag', *Constr. Build. Mater.*, vol. 25, no. 2, pp. 1018–1025, 2011, doi: https://doi.org/10.1016/j.conbuildmat.2010.06.077.

[12] J. Shi-Ping and J. Grandet, 'Evolution comparee des porosites des mortiers de ciment au laitier et des mortiers de ciment portland', *Cem. Concr. Res.*, vol. 19, no. 3, pp. 487–496, 1989, doi: https://doi.org/10.1016/0008-8846(89)90037-9.

[13] T. Merzouki, M. Bouasker, N. E. H. Khalifa, and P. Mounanga, 'Contribution to the modeling of hydration and chemical shrinkage of slag-blended cement at early age', *Constr. Build. Mater.*, vol. 44, pp. 368–380, 2013, doi: https://doi.org/10.1016/j.conbuildmat.2013.02.022.

[14] T. Knudsen, 'The dispersion model for hydration of Portland cement I. General concepts', *Cem. Concr. Res.*, vol. 14, no. 5, pp. 622–630, 1984.

[15] B. Kolani, L. Buffo-Lacarrière, A. Sellier, G. Escadeillas, L. Boutillon, and L. Linger, 'Hydration of slag-blended cements', *Cem. Concr. Compos.*, vol. 34, no. 9, pp. 1009–1018, 2012.

[16] L. Kolani Batian ;. Escadeillas, Gilles ;. Sellier, Alain ;. Lacarrière, 'Comportement au jeune âge des structures en béton armé à base de liants composés aux laitiers', PhD Thesis, 2012. [Online]. Available: http://www.sudoc.fr/168945223

[17] Y. Elakneswaran, E. Owaki, S. Miyahara, M. Ogino, T. Maruya, and T. Nawa, 'Hydration study of slag-blended cement based on thermodynamic considerations', *Constr. Build. Mater.*, vol. 124, pp. 615–625, 2016, doi: https://doi.org/10.1016/j.conbuildmat.2016.07.138.

[18] L. Parrot and D. C. Killoh, ‘Prediction of cement hydration’, presented at the Proceedings of the British Ceramic Society, 1984, pp. 41–53.

[19] X.-Y. Wang, H.-S. Lee, K.-B. Park, J.-J. Kim, and J. S. Golden, ‘A multi-phase kinetic model to simulate hydration of slag–cement blends’, *Cem. Concr. Compos.*, vol. 32, no. 6, pp. 468–477, 2010, doi: https://doi.org/10.1016/j.cemconcomp.2010.03.006.

[20] X.-Y. Wang, ‘Analysis of hydration kinetics and strength progress in cement–slag binary composites’, *J. Build. Eng.*, vol. 35, p. 101810, 2021.

[21] L. Han-Seung and X.-Y. Wang, ‘Evaluation of compressive strength development and carbonation depth of high volume slag-blended concrete’, *Constr. Build. Mater.*, vol. 124, pp. 45–54, 2016.

[22] K.-B. Park, Y.-S. Wang, and X.-Y. Wang, ‘Property Analysis of Slag Composite Concrete Using a Kinetic–Thermodynamic Hydration Model’, *Appl. Sci.*, vol. 11, no. 16, p. 7191, 2021.

[23] T. Wagner, D. Kulik, F. Hingerl, and S. Dmytrieva, ‘GEM-Selektor Geochemical Modeling Package: TSolMod Library and Data Interface for Multicomponent Phase Models’, *Can. Mineral.*, vol. 50, pp. 1173–1195, Dec. 2012, doi: 10.3749/canmin.50.5.1173.

[24] W. Chen and H. J. H. Brouwers, ‘The hydration of slag, part 2: reaction models for blended cement’, *J. Mater. Sci.*, vol. 42, no. 2, pp. 444–464, Jan. 2007, doi: 10.1007/s10853-006-0874-1.

[25] M. Königsberger and J. Carette, ‘Validated hydration model for slag-blended cement based on calorimetry measurements’, *Cem. Concr. Res.*, vol. 128, p. 105950, Feb. 2020, doi: 10.1016/j.cemconres.2019.105950.

[26] H. M. Jennings and S. K. Johnson, ‘Simulation of microstructure development during the hydration of a cement compound’, *J. Am. Ceram. Soc.*, vol. 69, no. 11, pp. 790–795, 1986.

[27] P. Navi and C. Pignat, ‘Simulation of cement hydration and the connectivity of the capillary pore space’, *Adv. Cem. Based Mater.*, vol. 4, no. 2, pp. 58–67, 1996.

[28] K. Van Breugel, ‘Numerical simulation of hydration and microstructural development in hardening cement-based materials (I) theory’, *Cem. Concr. Res.*, vol. 25, no. 2, pp. 319–331, 1995.

[29] J. W. Bullard, ‘A three-dimensional microstructural model of reactions and transport in aqueous mineral systems’, *Model. Simul. Mater. Sci. Eng.*, vol. 15, no. 7, p. 711, 2007.

[30] S. Bishnoi and K. L. Scrivener, ‘μic: A new platform for modelling the hydration of cements’, *Cem. Concr. Res.*, vol. 39, no. 4, pp. 266–274, 2009.

[31] D. A. Kulik, F. Winnefeld, A. Kulik, G. D. Miron, and B. Lothenbach, ‘CemGEMS–an easy-to-use web application for thermodynamic modelling of cementitious materials’, *RILEM Tech. Lett.*, vol. 6, pp. 36–52, 2021.

[32] D. P. Bentz and D. P. Bentz, *CEMHYD3D: A three-dimensional cement hydration and microstructure development modelling package. Version 2.0*. US Department of Commerce, National Institute of Standards and Technology, 2000.

[33] J. W. Bullard, ‘Virtual cement and concrete testing laboratory: Version 9.5 user guide’, 2014.

[34] J. Atallah, H. Ranaivomanana, F. Bignonnet, and S. Bonnet, ‘A Benchmarking of Slag Blended Cement Hydration Models’, 2023, pp. 23–33. doi: 10.1007/978-3-031-33211-1_2.

[35] G. De Schutter and L. Taerwe, 'Degree of hydration-based description of mechanical properties of early age concrete', *Mater. Struct.*, vol. 29, no. 6, pp. 335–344, Jul. 1996, doi: 10.1007/BF02486341.

[36] A. Darquennes, B. Espion, and S. Staquet, 'How to assess the hydration of slag cement concretes?', *Constr. Build. Mater.*, vol. 40, pp. 1012–1020, 2013, doi: https://doi.org/10.1016/j.conbuildmat.2012.09.087.

[37] L. Wang, H. Q. Yang, S. H. Zhou, E. Chen, and S. W. Tang, 'Hydration, mechanical property and C-S-H structure of early-strength low-heat cement-based materials', *Mater. Lett.*, vol. 217, pp. 151–154, 2018, doi: https://doi.org/10.1016/j.matlet.2018.01.077.

[38] H. Y. Wang, 'The effects of elevated temperature on cement paste containing GGBFS', *Cem. Concr. Compos.*, vol. 30, no. 10, pp. 992–999, Nov. 2008, doi: 10.1016/j.cemconcomp.2007.12.003.

[39] C. Zemri and M. B. Bouiadjra, 'Comparison between physical–mechanical properties of mortar made with Portland cement (CEMI) and slag cement (CEMIII) subjected to elevated temperature', *Case Stud. Constr. Mater.*, vol. 12, p. e00339, 2020, doi: https://doi.org/10.1016/j.cscm.2020.e00339.

[40] N. E. H. Khalifa, M. Bouasker, P. Mounanga, and N. Benkahla, 'Physicochemical study of cementitious materials based on binary and ternary binders', *Chem. Mater. Res.*, vol. 4, p. 24, 2013.

[41] B. Vakhshouri and S. Nejadi, 'Empirical models and design codes in prediction of modulus of elasticity of concrete', *Front. Struct. Civ. Eng.*, vol. 13, pp. 38–48, 2019.

[42] W. Lang, Z. Liping, and T. Jian, 'Hydration Kinetics Model of Slag-blended Cement System', *IOP Conf. Ser. Earth Environ. Sci.*, vol. 242, p. 062074, Mar. 2019, doi: 10.1088/1755-1315/242/6/062074.

[43] S. Stephant, L. Chomat, A. Nonat, and T. Charpentier, 'Study of the hydration of cement with high slag content', presented at the 34th annual cement and concrete science conference, 2014.

[44] W. Deboucha, N. Leklou, A. Khelidj, and M. N. Oudjit, 'Hydration development of mineral additives blended cement using thermogravimetric analysis (TGA): Methodology of calculating the degree of hydration', *Constr. Build. Mater.*, vol. 146, pp. 687–701, Aug. 2017, doi: 10.1016/j.conbuildmat.2017.04.132.

[45] A. M. de Oliveira, A. P. Oliveira, J. D. Vieira, A. N. Junior, and O. Cascudo, 'Study of the development of hydration of ternary cement pastes using X-ray computed microtomography, XRD-Rietveld method, TG/DTG, DSC, calorimetry and FTIR techniques', *J. Build. Eng.*, vol. 64, p. 105616, 2023, doi: https://doi.org/10.1016/j.jobe.2022.105616.

[46] M. Avrami, 'Kinetics of phase change. I General theory', *J. Chem. Phys.*, vol. 7, no. 12, pp. 1103–1112, 1939.

[47] M. Avrami, 'Kinetics of Phase Change. II Transformation-Time Relations for Random Distribution of Nuclei', *J. Chem. Phys.*, vol. 8, no. 2, pp. 212–224, 1940, doi: 10.1063/1.1750631.

[48] M. Avrami, 'Granulation, Phase Change, and Microstructure Kinetics of Phase Change. III', *J. Chem. Phys.*, vol. 9, no. 2, pp. 177–184, 1941, doi: 10.1063/1.1750872.

[49] P. D. Tennis and H. M. Jennings, ‘A model for two types of calcium silicate hydrate in the microstructure of Portland cement pastes’, *Cem. Concr. Res.*, vol. 30, no. 6, pp. 855–863, 2000, doi: https://doi.org/10.1016/S0008-8846(00)00257-X.

[50] R. Berliner, M. Popovici, K. Herwig, M. Berliner, H. Jennings, and J. Thomas, ‘Quasielastic neutron scattering study of the effect of water-to-cement ratio on the hydration kinetics of tricalcium silicate’, *Cem. Concr. Res.*, vol. 28, no. 2, pp. 231–243, 1998.

[51] J. Biernacki, J. Richardson, P. Stutzman, and D. Bentz, ‘Kinetics of slag hydration in the presence of calcium hydroxide’, *J. Am. Ceram. Soc.*, vol. 85, no. 9, pp. 2261–2267, 2002.

[52] P. W. Brown, J. Pommersheim, and G. Frohnsdorff, ‘A kinetic model for the hydration of tricalcium silicate’, *Cem. Concr. Res.*, vol. 15, no. 1, pp. 35–41, 1985.

[53] M. Tarrida, M. Madon, B. Le Rolland, and P. Colombet, ‘An in-situ Raman spectroscopy study of the hydration of tricalcium silicate’, *Adv. Cem. Based Mater.*, vol. 2, no. 1, pp. 15–20, 1995.

[54] V. Waller, ‘Relations entre composition des betons, exothermie en cours de prise et resistance en compression’, PhD Thesis, 1999. [Online]. Available: http://www.theses.fr/1999ENPC9909/document

[55] I. G. Richardson, ‘The nature of C-S-H in hardened cements’, *Cem. Concr. Res.*, vol. 29, no. 8, pp. 1131–1147, 1999, doi: https://doi.org/10.1016/S0008-8846(99)00168-4.

[56] H. J. H. Brouwers, ‘The work of Powers and Brownyard revisited: Part 1’, *Cem. Concr. Res.*, vol. 34, no. 9, pp. 1697–1716, 2004, doi: https://doi.org/10.1016/j.cemconres.2004.05.031.

[57] I. G. Richardson and G. W. Groves, ‘Microstructure and microanalysis of hardened cement pastes involving ground granulated blast-furnace slag’, *J. Mater. Sci.*, vol. 27, no. 22, pp. 6204–6212, Nov. 1992, doi: 10.1007/BF01133772.

[58] F. Adenot, ‘Durabilite du beton : caracterisation et modelisation des processus physiques et chimiques de degradation du ciment’, thesis, Orléans, 1992. Accessed: Dec. 30, 2021. [Online]. Available: http://www.theses.fr/1992ORLE2001

[59] H. F. W. Taylor, *Cement chemistry, 2nd edition*. 1997.

[60] NF EN 196-3, ‘Méthodes d’essai des ciments — Partie 3 : Détermination du temps de prise et de la stabilité’, 2017.

[61] V. Baroghel-Bouny, ‘Which toolkit for durability evaluation as regards chloride ingress into concrete? Part II: Development of a performance approach based on durability indicators and monitoring parameters’, in *Third International RILEM Workshop on Testing and Modeling Chloride Ingress into Concrete*, 2004, pp. 137–163.

[62] S. M. Monteagudo, A. Moragues, J. C. Gálvez, M. J. Casati, and E. Reyes, ‘The degree of hydration assessment of blended cement pastes by differential thermal and thermogravimetric analysis. Morphological evolution of the solid phases’, *Thermochim. Acta*, vol. 592, pp. 37–51, 2014, doi: https://doi.org/10.1016/j.tca.2014.08.008.

[63] J. I. Bhatty, ‘Hydration versus strength in a portland cement developed from domestic mineral wastes — a comparative study’, *Thermochim. Acta*, vol. 106, pp. 93–103, 1986, doi: https://doi.org/10.1016/0040-6031(86)85120-6.

[64] EN NF 206-1, ‘Concrete - Part 1: Specification, performance, production and conformity’, 2004.

[65] NF P18-305, ‘Ready-mixed concrete’, 1996.

[66] M. ALI AHMAD, H. RANAIVOMANANA, S. BONNET, P. BUTTIN, and V. LHOSTIS, ‘Thermogravimetry outputs on different BFS-blended cement paste formulations from 7 to 960 days’. 2023. doi: 10.17632/93ztc35ypy.1.

[67] R. Snellings *et al.*, ‘RILEM TC-238 SCM recommendation on hydration stoppage by solvent exchange for the study of hydrate assemblages’, *Mater. Struct.*, vol. 51, no. 6, p. 172, Dec. 2018, doi: 10.1617/s11527-018-1298-5.

[68] AFNOR, ‘Essai Pour Béton Durci—Essai de Porosité et de Masse Volumique—NF P18-459’, 2022.

[69] NF EN 196-1, ‘Méthodes d’essais des ciments-Partie 1: détermination des résistances mécaniques [Methods of testing cements–part 1: determination of mechanical strengths]’, 2006.

[70] NF EN ISO 12680-1, ‘Méthodes d’essai pour produits réfractaires – Partie 1 : détermination du module de Young dynamique (MOE) par excitation de vibration par impulsion’, 2007.

[71] F. Bellmann and J. Stark, ‘Activation of blast furnace slag by a new method’, *Cem. Concr. Res.*, vol. 39, no. 8, pp. 644–650, 2009, doi: https://doi.org/10.1016/j.cemconres.2009.05.012.

[72] D. P. Bentz, ‘Influence of water-to-cement ratio on hydration kinetics: simple models based on spatial considerations’, *Cem. Concr. Res.*, vol. 36, no. 2, pp. 238–244, 2006.

[73] A. Jamshidi, K. Kurumisawa, T. Nawa, and M. O. Hamzah, ‘Analysis of structural performance and sustainability of airport concrete pavements incorporating blast furnace slag’, *J. Clean. Prod.*, vol. 90, pp. 195–210, 2015.

[74] E. E. Berry, R. T. Hemmings, M.-H. Zhang, B. J. Cornelius, and D. M. Golden, ‘Hydration in high-volume fly ash concrete binders’, *Mater. J.*, vol. 91, no. 4, pp. 382–389, 1994.

[75] F. M. Lea, ‘The chemistry of cement and concrete’, 1935.

[76] Y. Zhao, J. Gao, Z. Xu, S. Li, X. Luo, and G. Chen, ‘Long-term hydration and microstructure evolution of blended cement containing ground granulated blast furnace slag and waste clay brick’, *Cem. Concr. Compos.*, vol. 118, p. 103982, 2021, doi: https://doi.org/10.1016/j.cemconcomp.2021.103982.

[77] M. Whittaker, M. Zajac, M. B. Haha, F. Bullerjahn, and L. Black, ‘The role of the alumina content of slag, plus the presence of additional sulfate on the hydration and microstructure of Portland cement-slag blends’, *Cem. Concr. Res.*, vol. 66, pp. 91–101, 2014, doi: https://doi.org/10.1016/j.cemconres.2014.07.018.

[78] V. Kocaba, E. Gallucci, and K. L. Scrivener, ‘Methods for determination of degree of reaction of slag in blended cement pastes’, *Cem. Concr. Res.*, vol. 42, no. 3, pp. 511–525, 2012.

[79] S. Stephant, ‘Etude de l’influence de l’hydratation des laitiers sur les propriétés de transfert gazeux dans les matériaux cimentaires’, PhD Thesis, 2015. [Online]. Available: http://www.theses.fr/2015DIJOS090/document

[80] S. Song, D. Sohn, H. Jennings, and T. Mason, ‘Hydration of Alkali-Activated Ground Granulated Blast Furnace Slag’, *J. Mater. Sci.*, vol. 35, pp. 249–257, Jan. 2000, doi: 10.1023/A:1004742027117.

[81] Y. Zhang, G. Ye, and Z. Yang, 'Pore size dependent connectivity and ionic transport in saturated cementitious materials', *Constr. Build. Mater.*, vol. 238, p. 117680, 2020, doi: https://doi.org/10.1016/j.conbuildmat.2019.117680.

[82] H. M. Jennings, 'A model for the microstructure of calcium silicate hydrate in cement paste', *Cem. Concr. Res.*, vol. 30, no. 1, pp. 101–116, 2000, doi: https://doi.org/10.1016/S0008-8846(99)00209-4.

[83] D. P. Bentz, D. A. Quenard, V. Baroghel-Bouny, E. J. Garboczi, and H. M. Jennings, 'Modelling drying shrinkage of cement paste and mortar Part 1. Structural models from nanometres to millimetres', *Mater. Struct.*, vol. 28, no. 8, pp. 450–458, Oct. 1995, doi: 10.1007/BF02473164.

[84] O. Mohamed, 'Durability and Compressive Strength of High Cement Replacement Ratio Self-Consolidating Concrete', *Buildings*, vol. 8, no. 11, 2018, doi: 10.3390/buildings8110153.

[85] L. Yu *et al.*, 'Identification of multi-scale homogeneity of blended cement concrete: macro performance, micro and meso structure', *J. Therm. Anal. Calorim.*, vol. 147, no. 19, pp. 10293–10304, 2022.

[86] X. Du, Z. Li, T. Tong, B. Li, and H. Liu, 'Isothermal Drying Process and its Effect on Compressive Strength of Concrete in Multiscale', *Appl. Sci.*, vol. 9, no. 19, p. 4015, 2019.

[87] F. U. A. Shaikh and A. Hosan, 'Effect of nano silica on compressive strength and microstructures of high volume blast furnace slag and high volume blast furnace slag-fly ash blended pastes', *Sustain. Mater. Technol.*, vol. 20, p. e00111, 2019, doi: https://doi.org/10.1016/j.susmat.2019.e00111.

[88] Y. Kellouche and A. Bougara, 'Analyse d'évolution de la réactivité du laitier d'El-Hadjar Par les essais thermogravimétriques'.

[89] T. Boubekeur, B. Boulekbache, and A. Makhelouf, 'Influence du laitier sur les propriétés des ciments à base de calcaire', Symposium International sur la Construction en Zone Sismique (SICZS_2010 …, 2010.

[90] Y. Li, Y. Liu, and R. Wang, 'Evaluation of the elastic modulus of concrete based on indentation test and multi-scale homogenization method', *J. Build. Eng.*, vol. 43, p. 102758, 2021, doi: https://doi.org/10.1016/j.jobe.2021.102758.

Appendix A

References	Slag hydration kinetic models
Merzouki et al. [13]	$\xi_{slg}(t) = \xi_{slg}^{u} \times \frac{k(t-t_0)^n}{1+k(t-t_0)^n}$
Elakneswaran et al. [17]	$\alpha_{sg} = [A * \ln(t) + b] \times S_{sg} \times \exp[-\frac{E_{sg}}{R} \times (\frac{1}{T} - \frac{1}{T0})]$
Wang [19]	$\frac{d\alpha_{SG}}{dt} = \frac{m_{CH}(t)}{P}\frac{W_{cap}(t)}{W}\frac{3\rho_w}{v_{SG}r_{SG0}\rho_{SG}}\frac{1}{\left(\frac{1}{k_{dSG}}\frac{r_{SG0}}{D_{eSG}}\right)+\frac{r_{SG0}}{D_{eSG}}(1-\alpha_{SG})^{\frac{-1}{3}}+\frac{1}{k_{rSG}}(1-\alpha_{SG})^{\frac{-2}{3}}}$

Slag hydration kinetic models reported in the literature

Appendix B

Table of symbols:

Symbol	Description
OPC	Ordinary Portland Cement
BFS	Blast Furnace Slag
W/B	water to binder ratio
f_c	fraction of OPC in the mix
f_s	fraction of BFS in the mix
P0	Cement paste with 100% OPC and 0% BFS
P30	Cement paste with 70% OPC and 30% BFS
P50	Cement paste with 50% OPC and 50% BFS
P80	Cement paste with 20% OPC and 80% BFS
CH	Portlandite $Ca(OH)_2$
AFt	Ettringite ($C_6A\bar{S}_3H_{32}$)
AFm	Monosulfoaluminate ($C_4A\bar{S}H_{12}$)
HEXA	Hexahydrate (C_3AH_6)
HT	Hydrotalcite (M_5AH_{13})
AH	Hydrogarnet (C_4AH_{13})
Gh	Gehlenite ($Ca_2Al_2SiO_7$)
CSH	Hydrated calcium silicate of clinker
CASH	Hydrated calcium and aluminum silicate of slag
$(-)_i$	parameter referring to the binder i
(-)sc	parameter referring to the slag in presence of the clinker
$(C/S)_c$	molar ratio of (C/S) of the hydrate CSH of clinker
$(C/S)_s$	molar ratio of (C/S) of the hydrate CASH of slag
$(C/S)_{sc}$	molar ratio of (C/S) of the hydrate CASH of slag in presence of clinker
$(H/S)_c$	water demand of the CSH of clinker
$(H/S)_s$	water demand of the CASH of slag
$(H/S)_{sc}$	water demand of CASH of slag in presence of the OPC
$(A/S)_{sc}$	molar ratio A/S of the hydrate CASH of slag in presence of clinker

Symbol	Unit	Description
Φ	-	water porosity
m_{sat}	g	saturated mass of the sample
m_{dry}	g	dry mass measured after drying at 105°C
m_{hydro}	g	hydrostatic mass (measured underwater)
α	-	Mean hydration degree
α_i	-	hydration degree of the binder i
S_i	-	parameter that describes the ability of the binder i particle to hydrate

n_i	-	parameter that describes the accessibility of the water to the binder i
D	-	parameter that depends on the cure type
m_{i0}	g	initial mass of the binder i
$m_{i,hydrated}$	g	hydrated mass of the binder i
$m_{i,non\text{-}hydrated}$	g	non-hydrated mass of the binder i
j_i	-	oxide in the binder i
$F_{j,i}$	%	percentage of each oxide j present in the binder i
M_j	g/mol	molar mass of the oxide j
$[C_i]$	mol	number of mols of the CaO issued from the chemical composition of the binder i
$[S_i]$	mol	number of mols of the SiO2 issued from the chemical composition of the binder i
$[A_i]$	mol	number of mols of the Al_2O_3 issued from the chemical composition of the binder i
$[\dot{S}_i]$	mol	number of mols of the SO_3 issued from the chemical composition of the binder i
$[M_i]$	mol	number of mols of the MgO issued from the chemical composition of the binder i
M_h	g/mol	molar mass of the hydrate h
$V_{m,h}$	mol/cm^3	molar volume of the hydrate h
$m_{h,i}$	g	mass of the hydrate h produced from the hydration of the binder i
$V_{h,i}$	cm^3	volume of the hydrate h produced from the hydration of the binder i

Appendix C

	M_h (g/mol)	ρ (g/cm^3)	V_m (cm^3/mol)
CH_c [59]	74	2.23	33.1
CSH_c [59]	196.5	2.23	88.1
Afm_c [59]	622	1.99	313
Aft_c [59]	1237	1.73	715
$(C3AH6)_c$ [59]	378	2.52	150
Ah_s [15]	668.4	1.8	371.33
HT_s [15]	645.5	1.8	358.12
Aft_s [15]	1255.3	1.78	707.04
CASH [15]	$(C/S)_{sc}(t)\times M_C + M_{Si} + (A/S)_{sc} \times M_A + (H/S)_{sc}(t)\times M_H$	[87,12+74,1*$(C/S)_{sc}$ (t)] / [38,42+33,05*$(C/S)_{sc}$ (t)] ([24])	M/ρ_{CASH}

Chemical characteristics of the hydrates

Appendix D

Age (days)	m_{sample} (mg)	Ld_h*m_B (105°C-400°C)	Ld_x*m_B (400°C-600°C)	Ld_c*m_B (600°C-800°C)
P0_7d	24.9998	1.2687	1.2455	0.5129
P0_28d	23	1.4127	1.1905	0.4041
P0_56d	22.9992	1.6697	1.1287	0.1681
P0_90d	23.9988	1.881	1.3197	0.2383
P0_180d	23.9993	1.8292	1.4395	0.4184
P0_360d	23.9991	2.023	1.3942	0.2339
P0_530d	24.9992	2.0612	1.3453	0.1904
P0_822d	23.9994	2.1531	1.2499	0.2949
P0_960d	24	1.1322	1.2757	0.2922
P30_7d	23.9984	1.0288	0.7902	0.2159
P30_28d	23.9986	1.4579	0.8374	0.1635
P30_56d	22.999	1.6917	0.6174	0.004
P30_90d	23.9991	1.9619	0.8933	0.1402
P30_180d	23.999	1.9438	0.8153	0.1102
P30_360d	23.9987	2.0989	0.805	0.1094
P30-530d	24.9988	2.3965	0.889	0.1312
P30_822d	23.9993	2.2898	0.7599	0.0553
P30_860d	23.9988	2.2663	0.9037	0.143
P30_960d	23.9993	2.206	0.9282	0.1949
P50_7d	23.9982	1.0411	0.6199	0.1777
P50_28d	23.999	1.3789	0.6234	0.1229
P50_56d	23.9989	1.4472	0.5457	0.247
P50_90d	23.999	2.0894	0.7428	0.1331
P50_180d	23.9988	1.6149	0.5834	0.1653
P50_360d	23.999	1.8626	0.5829	0.0654
P50_530d	23.9989	1.8965	0.6228	0.1007
P50_822d	23.9987	2.3865	0.7785	0.1134
P50_860d	23.999	2.1075	0.7085	0.1007
P50_960d	24.9989	2.0052	0.6477	0.0971
P80_7d	22.9979	0.7593	0.1834	0.0586
P80_28d	23.9984	0.9363	0.3091	0.0893
P80_56d	22.9984	1.0984	0.185	-0.005
P80_90d	22.9979	1.5682	0.3744	0.0916
P80-180d	23.9982	1.2476	0.2418	0.046
P80_360d	23.9984	1.1665	0.244	0.0151
P80_530d	22.9984	1.3275	0.5417	0.0058
P80_822d	23.9988	1.5143	0.177	0.2527
P80_860d	23.9994	1.5021	0.3671	0.097
P80_960d	23.9987	1.7343	0.4299	0.0845

TGA experimentally results required for the prediction of the hydration degree